

Copyright
by
Jackwon Kim
2004

The Dissertation Committee for Jaekwon Kim
certifies that this is the approved version of the following dissertation:

**Signal Detection for OFDM Systems
with Transmit Diversity**

Committee:

Edward J. Powers, Supervisor

Ronald E. Barr

Gustavo de Veciana

Brian L. Evans

Robert W. Heath Jr.

Baxter F. Womack

**Signal Detection for OFDM Systems
with Transmit Diversity**

by

Jaekwon Kim, B.S., M.S.

DISSERTATION

Presented to the Faculty of the Graduate School of
The University of Texas at Austin
in Partial Fulfillment
of the Requirements
for the Degree of

DOCTOR OF PHILOSOPHY

THE UNIVERSITY OF TEXAS AT AUSTIN

May 2004

Dedicated to my wife Eunjung Kam.

Acknowledgments

I thank God for letting me finish the dissertation. Jesus said “I am the vine; you are the branches. If a man remains in me and I in him, he will bear much fruit; apart from me you can do nothing (John 15:5).”

Given that I started my Ph.D. study in fall 2000, I passed the qualifying exam rather early in fall 2001. I thought I qualified as a Ph.D., which turned out to be false in next semester. It was summer 2002 when I realized that my academic level is so low that I can not finish my study successfully. I asked my wife what she would think if I want to quit. She said that it is O.K. to her, which was a big comfort. I thanked God for giving me a wife whose mind is is not materialistic.

I prayed to God if I have to go back home without Ph.D. I thought of my parents who would be disappointed if I quit. Being afraid of being rejected by others, I really wanted to be a Ph.D. even when I do not qualify. I said to God that I wanted to be a Ph.D. even when I lack basics. God let me think that I have only to start again from basics. The answer was very clear and I wanted to understand basics. I now think that the shortest path to obtain a Ph.D. is to understand basic things for sure. I started to study statistical digital signal processing, information theory, linear algebra, taking classes and self studying. It was not pleasant that I had to study basics when

I was supposed to write papers. It was Dec. 2003 when my first journal paper was accepted. Having my first journal paper accepted, I could get to know how to write papers. I have submitted eight journal papers by now. Regardless of acceptance and rejection of my papers in the future, I sincerely thank God who let me have the ability to conduct research.

I thank Dr. Edward J. Powers for his guidance as my academic supervisor. When a paper was rejected, he encouraged me saying “Do not be disappointed, your next paper is more likely to be accepted”. I thank Dr. Heath for helping me write my first journal paper, especially the introduction part. I now understand how difficult it is to help others to write his or her first journal paper. He was patient with me who could not understand his comments on the structure, transition between paragraphs, and other important aspects of the introduction. I thank all of my other committee members, a good instructor Gustavo de Veciana, kind reminder Brian L. Evans, a Texan Ronald E Barr. I thank Baxter F. Womack for hiring me as a EE464 teaching assistant in spring 2001. I thank my lab. mates, Byungchul, Hoojin, Hyunsoo, Kitaek, Taeung, Seyeong, Changyong, Yongjune, Takehyun for their friendship.

I feel obligated to thank my church Gu-Yuk members. When Sarah was born in October 2003, I thought about postponing my graduation because I could not find time to work. Thanks God for letting me have good church friends who sincerely helped my family in need. Without their help, I will not graduate in May 2004.

I want to be in Him and He in me so that I can bear much fruit in my

life. Wherever He leads me to work, I desire to bear much fruit, pleasing Him.

Signal Detection for OFDM Systems with Transmit Diversity

Publication No. _____

Jaekwon Kim, Ph.D.

The University of Texas at Austin, 2004

Supervisor: Edward J. Powers

Digital communication techniques have been developed and improved to provide high rate data transmission as well as transmission reliability. High rate data transmission necessitates communication over broadband frequency selective channels. Multi-carrier modulation systems such as orthogonal frequency division multiplexing (OFDM) have become very popular for broadband communication due in part to computationally efficient multi-carrier generation using the fast Fourier transform (FFT) and simple one-tap equalization. Examples of wireless Internet standards employing OFDM are IEEE 802.11a/g wireless LANs and IEEE 802.16a fixed wireless networks.

Recently, transmit diversity technique such as the Alamouti space-time block code involving multiple transmit antennas and possible multiple receive antennas has emerged as a promising method to improve transmission reliability. OFDM combined with transmit diversity is a promising means of achieving

high rate data transmission with transmission reliability. A main assumption of OFDM systems with space-time block codes such as the Alamouti code is a quasi-static channel, i.e., wireless channels do not change over two consecutive OFDM symbol periods. Unfortunately, wireless channels become time-variant due to Doppler spread when a mobile receiver moves, resulting in severe communications performance degradation.

This dissertation proposes three novel signal detection methods for OFDM systems with transmit diversity when the channels are time-variant: a decision directed receiver, a sequence estimation receiver, and a frequency domain block linear filtering receiver. Computer simulations demonstrate the computational efficiency of the proposed methods, comparing with previous approaches.

This dissertation also proposes an OFDM transmission method without cyclic prefix. Since cyclic prefix in OFDM systems is redundancy, bandwidth efficiency increases as the redundancy is eliminated. It is also shown that the equalization technique for OFDM systems without cyclic prefix can also be used for timing error correction in non-synchronized sampling discrete multi-tone (DMT) systems, a wireline counterpart of OFDM.

Table of Contents

Acknowledgments	v
Abstract	viii
List of Tables	xiii
List of Figures	xiv
Chapter 1. Introduction	1
1.1 Orthogonal Frequency Division Multiplexing Systems	4
1.2 Contributions and Organization of the Dissertation	8
1.3 Notation	10
Chapter 2. Previous Signal Detection Methods for OFDM Systems with Transmit Diversity	12
2.1 Introduction	12
2.2 OFDM with Transmit Diversity	19
2.3 The Alamouti Decoding Scheme	26
2.3.1 Signal Detection in Slow Fading Channels	26
2.3.2 Signal Detection in Fast Fading Channels	27
2.3.3 Numerical Examples	29
2.4 Time Domain Block Linear Filter	31
Chapter 3. Decision Directed Receiver	34
3.1 Decision Directed Receiver	34
3.2 Simulation Results	36
3.3 Conclusions	38

Chapter 4. Sequence Estimation Receivers	40
4.1 An MLSE Formulation	40
4.2 An SDFSE Scheme with an AT	43
4.3 An AESE Scheme	47
4.4 Computational Complexity	48
4.5 Simulation Results	50
4.6 Conclusions	55
Chapter 5. Frequency Domain Block Linear Filter	58
5.1 Block Diagonal Approximation	58
5.2 Frequency Domain Block Linear Filter	61
5.3 Receiver Combining for Multiple Receive Antennas	67
5.4 Complexity Comparison	68
5.5 Simulation Results	69
5.6 Conclusions	72
Chapter 6. Bandwidth Efficient OFDM Transmission	78
6.1 OFDM without Cyclic Prefix	78
6.2 Previous Iterative Signal Detection Method	79
6.3 Proposed Signal Detection Method	80
6.4 Simulation Results	82
6.5 Conclusions	84
Chapter 7. Non-Synchronized Sampling System	86
7.1 DMT with Non-Synchronized Sampling	86
7.2 Timing Error in Non-synchronized Sampling Systems	88
7.3 Proposed Timing Error Correction Scheme	89
7.4 Simulation Results	90
7.5 Conclusions	91
Chapter 8. Conclusions and Future Work	94
8.1 Conclusions	94
8.2 Future Work	95
8.2.1 Equalization for Multi-User OFDM Systems	95
8.2.2 Extension of SDFSE with an AT	98

Bibliography	99
Vita	112

List of Tables

4.1	Required number of metric calculations for an Alamouti code-word estimation in various symbol estimation schemes.	50
5.1	Complexity comparison of the FDBLF and the TDBLF.	69
5.2	Complexity ratio of the FDBLF to the TDBLF for various q	73

List of Figures

1.1	Block diagram of baseband equivalent OFDM systems.	5
1.2	Equivalent parallel system for OFDM.	7
1.3	The amplitude of subcarriers in the frequency domain. The effect of time domain rectangular windowing due to finite OFDM symbol period can be observed. The subcarriers in OFDM systems are overlapped in a bandwidth efficient way.	8
2.1	OFDM system with transmit diversity.	21
2.2	The relative significance of the two couplings caused by the time-variant channel, $10\log_{10}(\bar{\Psi}[k_0]/\bar{\Psi}[0])$ vs. k_0 , for $f_D = 297Hz$	30
2.3	The BER performance vs. SNR of the Alamouti decoding scheme for $f_D=50$ and $297Hz$	31
3.1	BER performance of the Alamouti decoding scheme and the proposed decision directed decoding scheme with $I = 1, 2$ when the Doppler frequency is $50Hz$	37
3.2	BER performance of the Alamouti decoding scheme and the proposed decision directed decoding scheme with $I = 1, 2$ when the Doppler frequency is $100Hz$	38
3.3	BER performance of the Alamouti decoding scheme and the proposed decision directed decoding scheme with $I = 1, 2$ when the Doppler frequency is $200Hz$	39
4.1	Block diagram of the proposed adaptive effort receiver. When the instantaneous channel time-variation is significant the SDFSE with AT is used, and when it is not significant the simple Alamouti decoding is used.	48
4.2	BER performance (perfect CSI) of the Alamouti Decoding, proposed SDFSE with an AT($q = 0, 1, 2$), the Time Domain MMSE.	53
4.3	BER performance (estimated CSI) of the Alamouti Decoding, proposed SDFSE with an AT($q = 0, 1, 2$), the Time Domain MMSE, and differential STBC (no CSI estimation is necessary).	54
4.4	Number of candidates in the proposed SDFSE with an AT ($q = 1$) for various SNR values. Estimated CSI is used.	55

4.5	Coded BER performance (estimated CSI) of the Alamouti Decoding, proposed SDFSE with an AT($q = 1, 2$), and the Time Domain MMSE. Convolutional coding of rate 1/2 is used in conjunction with a bit level interleaving.	56
4.6	BER performance (estimated CSI) of AESE with $T_{AESE}=0.3$ and 0.4, SDFSE with an AT($q = 1$), the time domain MMSE.	57
5.1	Illustration of a block diagonal approximation when $q = 1$. The entries that are significant but are approximated as 0 in the block diagonal approximation are denoted as circled crosses.	62
5.2	An Example of $ G(k, m) $, $0 \leq k, m \leq 2N - 1$	63
5.3	BER performance of the Alamouti decoding, the previous time domain block-linear filter, and the proposed frequency domain block-linear filter when ideal CSI is assumed to be known. Two transmit antennas and one receive antenna OFDM system.	74
5.4	BER performance of the Alamouti decoding, the previous time domain block-linear filter, and the proposed frequency domain block-linear filter when CSI is estimated. Two transmit antennas and one receive antenna OFDM system.	75
5.5	Coded BER performance (estimated CSI) of the Alamouti Decoding, proposed FDBLF($q = 1, 3, 4$), and the Time Domain MMSE. Convolutional coding of rate 1/2 is used in conjunction with a bit level interleaving.	76
5.6	BER performance of the Alamouti decoding, the previous time domain block-linear filter, and the proposed frequency domain block-linear filter when CSI is estimated. Two transmit antennas and two receive antennas OFDM system with maximal ratio receive combining (MRRC).	77
6.1	Block diagram of the proposed method for OFDM transmission without cyclic prefix.	81
6.2	Indoor channels used in Chapter 6 simulations.	82
6.3	Frequency selectivity of the indoor channels	83
6.4	SER performance of the previous RISIC and the proposed signal detection algorithm for OFDM systems without cyclic prefix when channel #1 is used.	84
6.5	SER performance of the previous RISIC and the proposed signal detection algorithm for OFDM systems without cyclic prefix when channel #2 is used.	85

6.6	SER performance of the previous RISIC and the proposed signal detection algorithm for OFDM systems without cyclic prefix when channel #3 is used.	85
7.1	Block diagram of synchronized sampling DMT systems.	87
7.2	Block diagram of non-synchronized sampling DMT systems.	88
7.3	NMSE comparison when $N = 512$, $SFO = 100ppm$	92
7.4	Recovered constellation when $N = 512$, $SFO=100ppm$ (a) frequency domain rotor, (b) proposed approach with $P = 8$	93
8.1	Illustration of multi-user OFDM when there exists 2 users.	96
8.2	Example of subchannel gains in multi-user OFDM systems. Subchannels are assumed to be allocated in the same manner as in Fig.8.1.	97

Chapter 1

Introduction

In addition to the existing tremendous amount of information on the Internet, digital data is generated by many personal devices such as digital cameras, digital camcorders, personal computers, scanners, and even mobile cell phones. Although the already huge amount of information is still growing, storage devices seem to be good enough. The examples of storage devices are computer hard discs, magnetic tape, compact disc (CD), CD recordable (CDR), CD rewritable (CDRW), digital versatile disc (DVD), DVD recordable (DVDR), DVD rewritable (DVDRW), universal serial bus (USB) 2.0 memory stick. Digital communication techniques have been developed and improved to move the above mentioned data from one place to another to be stored in a local storage device. With the growing amount of information to be accessed by people, however, it seems that the current data transmission techniques need to be more enhanced in terms of transmission reliability, transmission rate, power/bandwidth efficiency, and low complexity.

In this dissertation, multicarrier communication systems, in particular, orthogonal frequency division multiplexing (OFDM) systems, are addressed. OFDM systems utilize multiple complex exponentials as multiple carriers. The

idea of multichannel data transmission without inter-symbol interference and inter-channel interference was first conceived by Chang [1]. The performance of the idea was analyzed by Saltzberg [2]. An OFDM system was first implemented using analog oscillators and low pass filters in the 1960s by Porter, Zimmerman, and Kirsh [3][4]. However, its attractive features were not fully revealed until an all-digital implementation using the fast Fourier transform (FFT) was used by Weinstein, Ebert, and Bingham [5][6]. The idea of the cyclic prefix to eliminate the interference between consecutive OFDM symbols was proposed by Peled and Ruiz [7]. It was shown by Hirosaki [8] that orthogonally multiplexed QAM signals can be successfully transmitted using the discrete Fourier transform (DFT). The advantages of OFDM systems are summarized as follows

1. The use of the IFFT/FFT enables the computationally efficient generation of exactly orthogonal complex exponentials to be used as carriers, without using multiple analog oscillators.
2. Compared to previous FDM systems, OFDM systems achieve higher spectral efficiency because its subchannels are allowed to overlap without interference.
3. Compared to single carrier modulation systems in which the implementation complexity is dominated by equalization [9], OFDM equalization is simpler because a frequency selective channel is treated as a set of flat fading subchannels (one-tap equalization per subchannel).

4. Adaptive modulation according to the subchannel signal-to-noise ratio (SNR) is possible in relatively slow time-varying channels [9].

5. OFDM is robust against narrowband interference, because such interference affects only a small percentage of the subcarriers [9].

Due to these attractive features, OFDM or its wireline counterpart discrete multitone (DMT) modulation has been used for

1. Digital audio/video broadcasting (DAB/DVB) [10][11][12][9][13][14][15]

2. Asymmetric and very high-speed digital subscriber line (DSL) modems [16][17][18]

3. Digital cable television systems [19]

4. Local area mobile networks such as IEEE 802.11a and the HIPER-LAN/2 [20][21][22][23][24].

It is also likely to be used for

1. Ultra wideband (UWB) communication [25][26]

2. Future generation mobile cellular systems with an aid of multiple transmit and receive antennas [27].

The remainder of this chapter is organized as follows. Since various OFDM systems are addressed in the dissertation, conventional OFDM system with single transmit and single receive antenna is described in Section 1.1. I also point out major assumptions in conventional OFDM systems. Various OFDM systems are described in appropriate chapters. In Section 1.2, I describe my

contributions and the organization of the dissertation. Section 1.3 presents the notation that the dissertation uses.

1.1 Orthogonal Frequency Division Multiplexing Systems

A block diagram of baseband equivalent OFDM systems is shown in Fig. 1.1. A information bit stream is mapped into a complex symbol streams. A block of complex symbols is converted from serial to parallel (S/P) to be used as input to the inverse fast Fourier transform (IFFT). The modulated OFDM signal to be transmitted over a channel is expressed as

$$x_i[n] = \frac{1}{\sqrt{N}} \sum_{k=0}^{N-1} X_i[k] e^{j2\pi kn/N} \quad (1.1)$$

where $x_i[n]$, $0 \leq n \leq N - 1$, stands for the n -th sample in the i -th OFDM symbol and $X_i[k]$, $0 \leq k \leq N - 1$, is the transmitted complex data on the k -th subchannel during the i -th symbol period. The parameter N represents the number of subchannels. A cyclic extension is applied to the time domain symbol before transmission as

$$\tilde{x}_i[n] = x_i[(n + N - \nu)_N], -\nu \leq n \leq N - 1 \quad (1.2)$$

where $(n)_N$ is n modulo N . That is, a cyclic prefix of ν samples is prepended to the symbol. Transmit signal right before the transmit low pass filter can be represented in continuous time as

$$x(t) = \sum_{i=-\infty}^{\infty} \sum_{n=-\nu}^{N-1} \tilde{x}_i(nT_s) \delta(t - ((N + \nu)i + n)T_s) \quad (1.3)$$

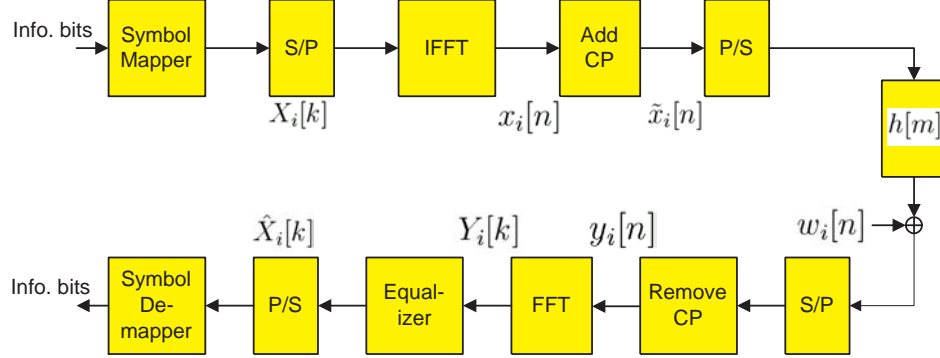


Figure 1.1: Block diagram of baseband equivalent OFDM systems.

where $x_i(nT_s) \triangleq x_i[n]$, T_s is the sampling period, and $\delta(t)$ is the Dirac Delta function.

The received signal after passing through an equivalent channel is expressed as

$$\begin{aligned}
 y(t) &= \int_{-\infty}^{\infty} h(\tau)x(\tau - t)d\tau \\
 &= \sum_{i=-\infty}^{\infty} \sum_{m=-\nu}^{N-1} \tilde{x}_i(mT_s)h(t - ((N + \nu)i + m)T_s). \quad (1.4)
 \end{aligned}$$

I assume that the equivalent channel impulse response including the transmit filter, wireless channel impulse response, and the receive filter, has a finite length, i.e., $h(t) = 0$ for $t < 0$ or $t > (M - 1)T_s$.

Sampled at the receiver, the i -th OFDM symbol after having the cyclic prefix removed is expressed as

$$y_i[n] = \sum_{m=0}^{M-1} h[m]x_i[(n - m)_N] + w_i[n], \quad 0 \leq n \leq N - 1 \quad (1.5)$$

where $h[m] \triangleq h(mT_s)$ and $w_i[n]$ is the additive white Gaussian noise during the i -th OFDM symbol period. In (1.5), it is assumed that $M - 1 \leq \nu$.

The received signal is converted into the frequency domain via a demodulating FFT :

$$Y_i[k] = \frac{1}{\sqrt{N}} \sum_{n=0}^{N-1} y_i[n] e^{-j2\pi kn/N}, \quad 0 \leq k \leq N - 1. \quad (1.6)$$

Since the received signal in (1.5) is the circular convolution of the transmitted signal and the channel impulse response, the frequency domain signal can also be expressed as

$$Y_i[k] = X_i[k] \cdot H[k] + W_i[k], \quad 0 \leq k \leq N - 1 \quad (1.7)$$

where $H[k]$ and $W_i[k]$ are the FFT result of $h[n]$ and $w_i[n]$, respectively.

Using the above relationship of the transmitted and the received signals in the frequency domain, the compensation for the channel distortion is performed by a one-tap equalizer for each tone, which estimates the transmitted symbols. Tones can be seen as independent of each other, which leads to an equivalent system illustrated in Fig. 1.2. Fig. 1.3 shows a set of subchannels in the frequency domain. It can be seen that the subchannels are overlapped in a bandwidth efficient manner.

Major Assumptions: The above conventional OFDM system assumes the following:

1. A linear time invariant (LTI) channel. If the channels are linear time variant (LTV), then the orthogonality between the subchannels is broken,

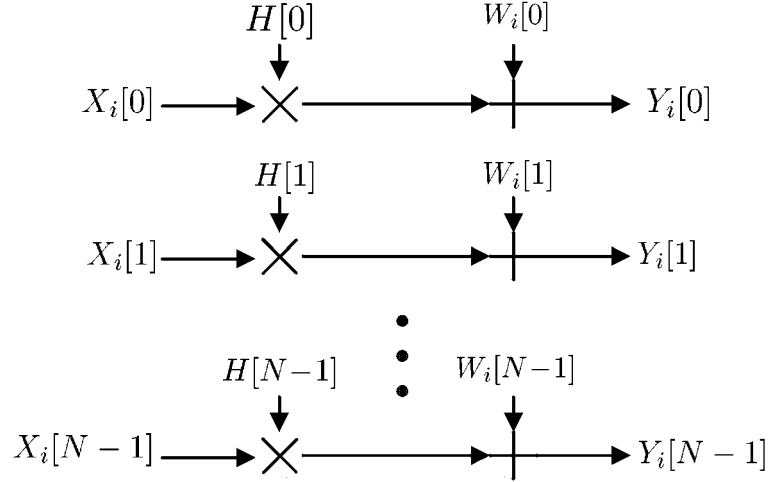


Figure 1.2: Equivalent parallel system for OFDM.

thereby degrading performance. The dissertation concerns OFDM systems with transmit diversity when the channel is LTV.

2. A cyclic extension that is longer than the channel impulse response to guarantee that there is no interference between OFDM symbols. However, a long cyclic prefix incurs bandwidth efficiency reduction because the cyclic extension is redundant. Therefore, this dissertation deals with OFDM systems without cyclic extension in an effort to increase the bandwidth efficiency in indoor wireless channels.

3. Perfect sampling time synchronization between the transmitter and the receiver. If sampling time is not correct at the receiver, the error needs to be corrected. The dissertation deals with timing error correction in non-synchronized sampling DMT systems.

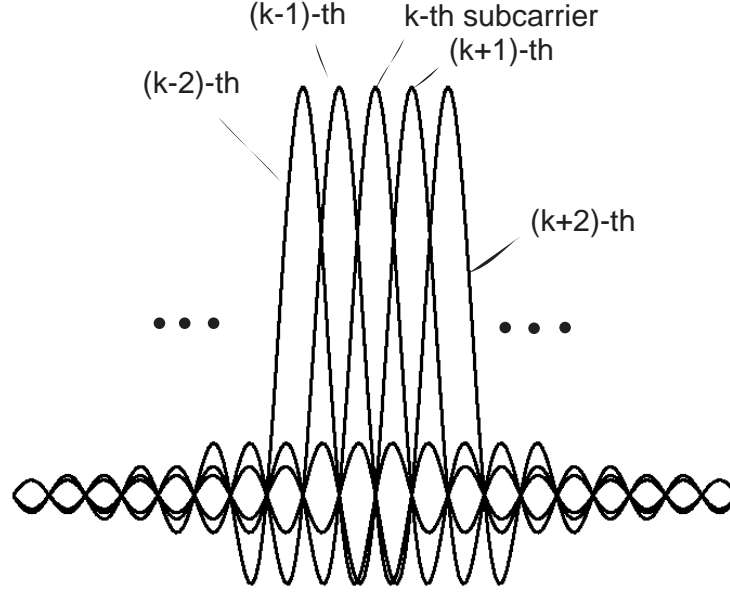


Figure 1.3: The amplitude of subcarriers in the frequency domain. The effect of time domain rectangular windowing due to finite OFDM symbol period can be observed. The subcarriers in OFDM systems are overlapped in a bandwidth efficient way.

1.2 Contributions and Organization of the Dissertation

My contributions are the following:

- I propose three types of receivers for OFDM systems with transmit diversity in fast fading channels, a decision directed receiver (Chapter 3), sequence estimation receivers (Chapter 4), and a frequency domain block-linear filtering receiver (Chapter 5) to mitigate the degrading effect of time variant channels.
- I show that the idea of subsymbol equalization can be successfully applied to OFDM transmission without cyclic prefix (Chapter 6) and timing error

correction in non-synchronized sampling OFDM (DMT) systems (Chapter 7).

The dissertation is organized as follows:

Chapter 2 motivates the need of new receivers for OFDM systems with transmit diversity when the channels are fast fading. Two previous signal detection methods are also described: the Alamouti decoding and time domain block linear filtering approach.

Chapter 3 proposes a new decision directed receiver for OFDM systems with transmit diversity in fast fading channels by assuming ideal channel state information (CSI) at the receiver. The new decision directed receiver compensates for the ICI using intermediate decisions.

Chapter 4 first formulates a maximum likelihood sequence estimation (MLSE) method and show that its complexity is quite high for OFDM systems with transmit diversity in fast fading channels. Then I show that sequential decision feedback sequence estimation (SDFSE) with an adaptive threshold (AT) offers a good trade-off between computational complexity and error performance. To further decrease the average complexity of the SDFSE with an AT, I propose an adaptive effort sequence estimation (AESE). The AESE is motivated by the observation that instantaneous channel variation is not always significant even when the normalized Doppler frequency is high.

Chapter 5 proposes a new frequency domain block linear filter (FDBLF) approach for the signal detection in OFDM systems with transmit diversity. The FDBLF is based on the observation that the system matrix in the fre-

quency domain is quite sparse.

Chapter 6 proposes a new bandwidth efficient OFDM systems without cyclic prefix. I describe a previous iterative method briefly. I then compare the two schemes under indoor wireless channel environments.

Chapter 7 applies the idea of subsymbol equalization, a technique used for OFDM without cyclic prefix in chapter 6, to non-synchronized sampling DMT systems. In non-synchronized sampling systems, a free running crystal is used for sampling time generation without feedback from the digital domain. Timing error caused by the crystal is corrected in the digital domain. It is shown that the idea of subsymbol equalization can also be successfully used for the timing error correction.

1.3 Notation

In general, a bold face letter stands for a matrix or a vector as is clear from context. The operation $wrev(\cdot)$ reverses the order of elements in the argument vector; $\{\cdot\} \setminus \{\cdot\}$ denotes the set minus; $(\cdot)^T$ stands for the matrix transpose; $(\cdot)^*$ denotes the complex conjugate; $Diag(\cdot)$ represents an $N \times N$ diagonal matrix whose diagonal entries correspond to the $N \times 1$ argument vector entries; $(\cdot)_N$ denotes the modulo operation; \mathbf{I}_M denotes $M \times M$ identity matrix; $(\cdot)^H$ denotes hermitian transpose; $|\cdot|$ denotes absolute value; $\|\cdot\|$ denotes L_2 norm of a matrix or a vector; if $\sigma \triangleq (a, b, \dots, z)$ is a sequence, $\sigma \setminus a = (b, c, \dots, z)$; the notation $(\mathbf{X}[m]|m \in \mathcal{K})$, where \mathcal{K} is a set, denotes a sequence whose element indices are increasingly ordered; $[\cdot]_k$ denotes the

k -th element of the argument vector; $[\cdot]_{k,m}$ denotes the (k,m) -th entry of the argument matrix.

Chapter 2

Previous Signal Detection Methods for OFDM Systems with Transmit Diversity

This chapter describes two previous signal detection methods for OFDM systems with transmit diversity in fast fading channels. Sec.2.1 introduces the signal detection in OFDM systems with transmit diversity. Note that Sec.2.1 is the introduction to Chapters 2 through 5. Sec.2.2 describes MIMO OFDM systems in detail. Then two previous signal detection methods are described in Sec.2.3 and Sec.2.4. The performance of the time domain block linear filter will be presented in chapters 4 and 5.

2.1 Introduction

In recent years, transmit diversity techniques have received attention because they increase transmission reliability over wireless fading channels without penalty in bandwidth efficiency [28][29]. Space-time coding at the transmitter does not require channel state information (CSI), thus no feedback from the receiver to the transmitter is necessary[30][31][32]. One popular and practical transmit diversity technique is the Alamouti scheme [33], in which maximum-likelihood decoding naturally decouples the signals transmit-

ted from different antennas. The simple Alamouti decoding scheme works well when channels are flat fading and time-invariant over an Alamouti codeword period.

Unfortunately, high data rate applications necessitate data transmission over broadband frequency selective channels, which cause severe inter-symbol interference (ISI). However, a frequency selective channel can be divided into a set of parallel flat fading channels by combining the Alamouti technique with orthogonal frequency division multiplexing (OFDM) modulation method [34]-[35]. In these Alamouti coded OFDM systems, the simple Alamouti decoding at each subchannel requires that channels be constant over two OFDM symbol periods. When the quasi-static channel condition is met and an appropriate cyclic prefix (CP) is used, the simple Alamouti decoding works well.

The combination of Alamouti technique and OFDM modulation, however, makes the degrading time-varying channel effects more severe. Since OFDM systems have a much longer symbol duration than single carrier systems, a channel that is quasi-static for single carrier systems may not be quasi-static for OFDM systems. Consequently, rapidly changing channels cause more severe performance degradation in the Alamouti coded OFDM systems than in Alamouti coded single carrier systems. When the channel is fast fading, channel variation within an OFDM symbol gives rise to inter-channel interference (ICI) or coupling between the symbols in different codewords (inter-codeword coupling). In addition, the channel variation between two consecutive OFDM

symbols causes coupling between symbols in a codeword at each subchannel (intra-codeword coupling). With the two coupling effects lowering the effective signal-to-noise ratio (SNR) at the receiver, as will be shown in Sec. 2.3.3, the Alamouti decoding performance is degraded significantly in a fast fading channel environment. The severe performance degradation motivates the need for a decoding scheme that improves the performance at moderate complexity.

The effect of fast fading channel on BER performance of OFDM systems was analyzed in [36], however, no transmit diversity technique was considered in [36]. Performance degradation due to fast fading channels in systems with transmit diversity using the Alamouti code was considered in [37]. Since a single carrier system was considered in [37], however, ICI was not included as a performance degrading factor. In [38], a new model of signal to interference plus noise ratio (SINR) in multiple input multiple output (MIMO) OFDM system, including the impact of time-varying channel was proposed. In this chapter, I separate the impact of time-varying channel into the inter-codeword and intra-codeword coupling (both are defined in Sec. 2.3.2), and use them to analyze the effect of channel variation within an OFDM symbol period.

Various decoding schemes for space-time coded systems have been proposed. In [39], it was reported that transmit diversity exploiting the Alamouti code and its simple decoding can be used for a single carrier system even when channels are not quasi-static. This is possible due in part to a relatively short symbol period of single carrier systems when compared with OFDM systems. In [40], a simplified maximum likelihood (ML) decoder for space-

time block coded single carrier system was proposed when channels are time-selective. A decoding matrix was proposed in an effort to make the resultant matrix (channel matrix multiplied by the decoding matrix) diagonal, eliminating inter-antenna interference. An adaptive frequency domain equalization scheme was also proposed for single carrier systems in [41] to track channel variations within a transmission block. The previous approaches [39]-[41] consider single carrier systems, where interchannel interference is not applicable, thus these approaches do not apply to OFDM systems.

Decoding schemes in OFDM systems with transmit diversity were reported in [38][42][43]. A time domain filtering approach was proposed in [38] for MIMO OFDM systems in fast fading channels. I compare our proposed approaches mainly with this previous approach. In [38], a time-variant filter is designed in the time domain so that SINR including channel variation effect is maximized. As will be shown in detail later, however, the design process as well as filtering process is computationally expensive for some system parameters. In [42], a space-frequency encoding/decoding scheme for wideband OFDM system was proposed to improve performance, concatenating space-time block coding with trellis coded modulation (thereby increasing complexity). However, [42] assumes a slow-fading channel, which is not the case I consider in the Chapters 2-5. OFDM systems with ICI and ISI were considered in [43] and a decision feedback equalization (DFE) structured equalizer was developed. But the ICI considered in [43] is due to insufficient CP length rather than fast fading channels.

A differential space-time block coding (STBC) scheme was developed based on the Alamouti scheme in [44], eliminating the need for channel estimation. The differential scheme becomes relatively more bandwidth efficient (when compared with a coherent scheme) in fast fading channels because no training symbol is required to estimate the channels. The differential scheme, however, assumes that the channels do not change over two Alamouti codeword periods, i.e., four OFDM symbol periods, which is not true under the fast fading channels under consideration. Therefore, the fast time variation of the channels is likely to have a more severe impact on performance of differential space-time block coded systems than on coherent systems. I compare the performance of the proposed receivers with the differentially coded system through simulations at a high Doppler and show the advantages of coherent approaches in Sec. 4.5. Although more thorough comparison could be made considering different Doppler frequencies and different CSI estimation schemes, I consider only a fixed high Doppler frequency and one CSI estimation scheme.

In this chapter, I analyze the inter-codeword and intra-codeword coupling effects and demonstrate their severity via simulation. The previous time domain MMSE receiver is described in detail.

In Chapter 3, a decision directed receiver is proposed to mitigate the performance degradation due to fast fading channels. In the decision directed receiver, intermediate decisions are made to be used for interference cancellation between subchannels.

In Chapter 4, I use sequence estimation schemes [45]-[46] that are tra-

ditionally single carrier equalization techniques to alleviate the performance degradation due to the coupling effects. First, I formulate a maximum-likelihood sequence estimation (MLSE) scheme in the frequency domain. In [47], it was argued that small normalized Doppler frequency (the product of the Doppler frequency and symbol period) implies that ICI is from only a few nearest subchannels. In the MLSE formulation, I take advantage of an observation that even when the normalized Doppler frequency is somewhat large, I need to compensate for ICI from only a few nearest subchannels because of channel estimation error as well as less significance of ICI from far away subchannels. Second, a sequential decision feedback sequence estimation (SDFSE) scheme is described as a suboptimal scheme that reduces the high computational complexity of the MLSE. The complexity of the SDFSE scheme is again reduced by using an adaptive threshold (AT). Twice the inter-codeword coupling, which will be defined later, is used as a threshold value. The SDFSE scheme with an AT is composed of candidate selection step and sequence estimation step. The applicability of the AT idea is based on the observation that the inter-codeword coupling is much weaker than the intra-codeword coupling. The relatively small inter-codeword coupling keeps the number of candidates small to make efficient the SDFSE with an AT.

To further reduce the average complexity of the SDFSE with an AT, I propose an adaptive effort symbol estimation (AESE) scheme. Basically, the simple Alamouti decoding scheme is selected when the instantaneous channel variation is negligible, and the SDFSE scheme with an AT is used when

the channel variation is significant. The degree of the channel variation is measured in terms of intra-codeword coupling which is defined later. When the intra-codeword coupling is larger than a certain threshold, instantaneous channel variation is considered as significant, and vice versa. The threshold value in the AESE is set from simulation experiments. The AESE scheme is motivated by the observation that a high Doppler frequency does not necessarily mean an instantaneous significant channel variation. Therefore, even when the Doppler frequency is very high, transmitted symbols are estimated via the Alamouti decoding when the instantaneous channel variation is negligible. The Alamouti decoding, the SDFSE with an AT, the AESE, and the time domain MMSE filter approach are compared in terms of complexity and performance via simulation. Since each signal estimation scheme may react differently to channel estimation errors, I consider both cases with and without ideal CSI. I use the channel estimation technique involving pilot tones and interpolation in [38] to estimate CSI.

The main drawbacks of the sequence estimation, however, are that the complexity is time-variant that is not amenable to hardware implementation, and that the complexity is dependent on the constellation size.

In Chapter 5, a frequency domain block-linear filter (FDBLF) is proposed whose length is much shorter than the previous TDBLF, thereby achieving a significant complexity reduction in filter design as well as filtering process. The proposed FDBLF complexity is neither time-variant nor depends on constellation size. First, I extend the block diagonal approximation of system

matrix of single-input single-output (SISO) systems [47] to MIMO cases. I then use the extended block diagonal approximation to divide a large system equation into a set of small system equations. Then I formulate an optimization problem that is similar to [38] for each small system equation. It is shown that the FDBLF is computationally much more efficient than the previous TDBLF. The two approaches are also compared in terms of error performance versus signal-to-noise ratio (SNR). Monte Carlo simulations suggest that the proposed FDBLF shows a negligible performance degradation while requiring much less computations, compared with the previous TDBLF. It is also shown that the error performance gap between the two schemes becomes even smaller when CSI estimation error is included.

It is also shown that the simple Alamouti decoding might be a preferred choice even in very fast fading channels, depending on target BER, the cost of an additional radio frequency (RF) chain, and computational complexity. At BER of 10^{-3} , the simple Alamouti decoding (employing two transmit and two receive antenna) requires about $5.5dB$ less SNR than the quite complex time domain filtering approach (employing two transmit and one receive antenna).

2.2 OFDM with Transmit Diversity

In Chapters 2-5, I consider an OFDM system with transmit diversity as illustrated in Fig. 2.1. The bandwidth ($B = \frac{1}{T_s}$) is divided into N equally spaced subcarriers at frequencies $k\Delta f$, $k = 0, 1, \dots, N - 1$ with $\Delta f = B/N$ and T_s is the sampling interval. At the transmitter, information

bits are grouped and mapped into complex symbols. In the Chapters 2-5, quaternary phase-shift keying (QPSK) with constellation C_{QPSK} is assumed for the symbol mapping. According to the Alamouti code, $[X_1[k] \ X_2[k]]$ are transmitted from the two antennnas simultaneously during the first symbol period ($l = 1$) for each $k \in \mathcal{K}$. During the second symbol period ($l = 2$), $[-X_2^*[k] \ X_1^*[k]]$ are transmitted from the two antennas for each $k \in \mathcal{K}$. The set $\mathcal{K} \triangleq \{\frac{N-N_c}{2}, \dots, \frac{N+N_c}{2} - 1\}$ is the set of data carrying subcarrier indices; N_c is the number of subcarriers carrying data; N is the fast Fourier transform (FFT) size; and consequently the number of virtual carriers is $N - N_c$. I assume half of the virtual carriers are on both ends of the spectral band. The IFFT converts each $N \times 1$ complex vector into a time domain signal and the copy of the last D samples are appended as prefix (cyclic prefix). Thus the length of an OFDM symbol is $(N + D)T_s$. The time domain transmitted signals from antenna i during the l -th symbol period $x_{i,l}[n], 0 \leq n \leq N + D - 1$, $i \in \{1, 2\}$, $l \in \{1, 2\}$ are expressed as

$$x_{i,l}[n] = \sum_{k \in \mathcal{K}} S_{i,l}[k] e^{j2\pi k(n-D)/N} \quad (2.1)$$

where $S_{i,l}[k]$ denotes a complex symbol transmitted from the i -th antenna during the l -th symbol period in an Alamouti codeword over the k -th subchannel. The index for the Alamouti codeword is omitted to keep the notation simple.

The signals from the two transmit antennas go through independent channels.

Wireless Channels: The baseband wireless mobile channel impulse response

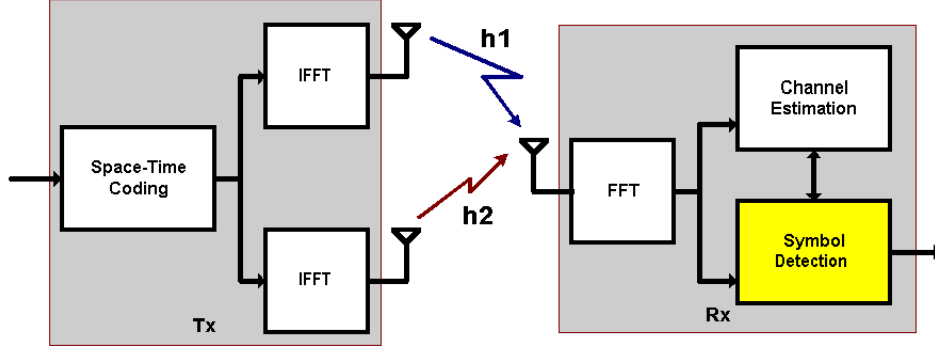


Figure 2.1: OFDM system with transmit diversity.

(CIR) can be expressed as [48]

$$h(t, \tau) = \sum_p \gamma_p(t) c(\tau - \tau_p) \quad (2.2)$$

where τ_p is the delay of the p -th path, $\gamma_p(t)$ is the corresponding complex amplitude, and $c(t)$ is the pulse shaping filter. The frequency response of the CIR at time t is

$$H(t, f) \triangleq \int_{-\infty}^{\infty} h(t, \tau) e^{-j2\pi f \tau} d\tau \quad (2.3)$$

$$= C(f) \sum_p \gamma_p(t) e^{-j2\pi f \tau_p} \quad (2.4)$$

where

$$C(f) \triangleq \int_{-\infty}^{\infty} \gamma_p(t) e^{-j2\pi f \tau} d\tau. \quad (2.5)$$

The frequency response of the shaping filter is usually a square-root raised-cosine Nyquist filter. From the property of Nyquist filter, $c(\tau - \tau_p) = \delta(\tau - \tau_p)$ if τ_p is a multiple of T_s . Therefore, discrete time equivalent channel impulse

response is

$$h[n, l] \triangleq h(nT_s, lT_s) = \sum_p \gamma_p[n] \delta[l - \tau_p'] \quad (2.6)$$

where $\gamma_p[n] \triangleq \gamma_p(nT_s)$ and $\delta[l - \tau_p'] \triangleq \delta(lT_s - \frac{\tau_p}{T_s})$.

When τ_p is not a multiple of T_s , however, $c(\tau - \tau_p) \neq \delta(\tau - \tau_p)$. Hence,

$$h[n, l] = \sum_p \gamma_p[n] c[l - \tau_p']. \quad (2.7)$$

Note that τ_p' is not an integer and $c[l - \tau_p'] \neq 0$ for all l . The amplitude of $c[l - \tau_p']$ decreases as $|l - \tau_p'|$ increases. For an extreme case, I consider a single path channel, i.e., $h[n, l] = \gamma_p[n] c[l - \tau_p']$. Even when there exist a single path, its discrete time equivalent CIR can have multiple significant taps. This is important when CIR is estimated in the time domain, because the number of taps to be estimated needs to be decided prior to the estimation process. Channel estimation considering multipaths arriving at non-integer multiples of the symbol period is addressed in section V in[49].

Since I am focusing on signal detection rather than channel estimation, multipaths are assumed to arrive at multiples of the symbol period for simulation simplicity in the dissertation. Then the wireless channel can be described as L resolved multipath components $p \in \{0, 1, \dots, L-1\}$, each characterized by an amplitude $h_{i,l}[n, p]$ and a delay pT_s , where $h_{i,l}[n, p]$ stands for the p -th resolved multi-path component amplitude between the i -th transmit antenna and the receive antenna at time n (sample index) during the l -th symbol period. The maximum delay spread of the two channels is assumed to be the same and equal to $(L-1)T_s$.

The received signals during an Alamouti codeword period are

$$y_l[n] = \sum_{i=1}^2 \sum_{p=0}^{L-1} h_{i,l}[n,p] x_{i,l}[n-p] + z_l[n], \quad l \in \{1, 2\} \quad (2.8)$$

where $z_l[n]$ is a circularly symmetric zero-mean white complex Gaussian random process. In (2.8), I assume the followings

- Exact carrier frequency synchronization between the transmitter and the receiver is assumed.
- Exact sampling time synchronization is assumed. The effect of receive filter, usually a raised cosine filter, needs to be included when sampling time is not exact.
- Exact frame synchronization is assumed for OFDM demodulation block.
- Cyclic prefix length is assumed to be longer than the channel impulse response.
- No power control, therefore, equal power allocation among subchannels is assumed. Note that it is difficult to feedback CSI to transmitter under the fast fading channel environments.
- Multipath components are assumed to arrive with delays of multiple of symbol periods. Thus, no power leakage is assumed due to multi-paths arriving at a fraction of the symbol period.

It can be observed that the received signals are a superposition of signals from the two transmit antennas. If the CP length D is longer than $L - 1$, the received signals (2.8) (after removing the prefix) can be considered as the circular convolution result of the transmitted signals (2.1) and the channel.

Consequently, the demodulated signals in the frequency domain via the FFT are expressed as

$$Y_l[k] = \sum_{i=1}^2 \sum_{m \in \mathcal{K}} S_{i,l}[m] a_{i,l}[k, m] + Z_l[k], \quad l \in \{1, 2\} \quad (2.9)$$

where

$$a_{i,l}[k, m] \triangleq \sum_{p=0}^{L-1} H_{i,l,p}[k - m] e^{-j2\pi mp/N} \quad (2.10)$$

$$H_{i,l,p}[k - m] \triangleq \frac{1}{N} \sum_{n=0}^{N-1} h_{i,l}[n, p] e^{-j2\pi(k-m)n/N}. \quad (2.11)$$

The notation $H_{i,l,p}[k - m]$ represents the FFT of the p -th multipath component between the i -th transmit antenna and the receive antenna during the l -th symbol period. Note that $a_{i,l}[k, m], m \neq k$ denotes the ICI from the m -th subchannel to the k -th subchannel for each transmit antenna index $i \in \{1, 2\}$ and symbol period $l \in \{1, 2\}$. Additional interpretation of $H_{i,l,p}[k - m]$ and $a_{i,l}[k, m]$ is provided in [47].

The input output relationship (2.9) can also be cast into a matrix form as follows

$$\underbrace{\begin{bmatrix} \mathbf{Y}_1 \\ \mathbf{Y}_2^* \end{bmatrix}}_{\triangleq \mathbf{Y}} = \mathbf{Q}^{(Rx)} \underbrace{\begin{bmatrix} H_{11} \mathbf{Q}^H & H_{21} \mathbf{Q}^H \\ H_{22}^* \mathbf{Q} & -H_{12}^* \mathbf{Q} \end{bmatrix}}_{\triangleq \mathbf{H}} \underbrace{\begin{bmatrix} \mathbf{X}_1 \\ \mathbf{X}_2 \end{bmatrix}}_{\triangleq \mathbf{X}} + \underbrace{\begin{bmatrix} \mathbf{Z}_1 \\ \mathbf{Z}_2^* \end{bmatrix}}_{\triangleq \mathbf{Z}} \quad (2.12)$$

where $\mathbf{X}_i \triangleq [X_i(0) \ X_i(1) \ \cdots \ X_i(N-1)]^T$, $i = 1, 2$

$$\mathbf{Y}_l \triangleq [Y_l(0) \ Y_l(1) \ \cdots \ Y_l(N-1)]^T, \quad l = 1, 2$$

$$\mathbf{Z}_l \triangleq [Z_l(0) \ Z_l(1) \ \cdots \ Z_l(N-1)]^T, \quad l = 1, 2$$

$$\mathbf{Q}^{(Rx)} \triangleq \text{Diag}(\mathbf{Q}, \mathbf{Q}^H)$$

$$H_{i,l} \triangleq \begin{bmatrix} h_{i,l}(0;0) & 0 & \cdots & h_{i,l}(0;L-1) & \cdots & h_{i,l}(0;1) \\ \vdots & \vdots & \ddots & \ddots & \vdots & \vdots \\ 0 & \cdots & h_{i,l}(N-1;L-1) & \cdots & h_{i,l}(N-1;0) \end{bmatrix}.$$

The Toeplitz channel matrix $H_{i,l}$ describes the channel between the i -th transmit antenna and the receive antenna during the l -th symbol period. The matrix \mathbf{Q} is the $N \times N$ FFT matrix whose the (m, n) -th entry is $Q(m, n) = \frac{1}{\sqrt{N}} e^{-j2\pi mn/N}$, $0 \leq m, n \leq N-1$. The symbol $X_i(k)$ is the complex symbol transmitted over the k -th subchannel from the i -th transmit antenna during the first OFDM symbol period.

If the channels are quasi-static, the following is true

$$[\mathbf{Q}^{(Rx)} \mathbf{H}]_{k,m} \approx 0 \quad \text{if } (k)_N \neq (m)_N \quad (2.14)$$

where $(\cdot)_N$ denotes the modulo operation. Consequently, space-time decoding can be performed for each subchannel separately, using the simple Alamouti decoding.

When the channels are fast fading, however, the approximation (2.14) does not hold, leading to severe performance degradation of the Alamouti decoding. In the following sections, signal detection methods in fast fading channels are discussed.

Extension to more than one receive antenna system is straight forward where an appropriate combining scheme at the receiver would be necessary that is considered in Sec.5.3.

2.3 The Alamouti Decoding Scheme

In this section, the Alamouti decoding scheme is briefly reviewed under the assumption of a quasi-static channel. Then the performance degradation of the scheme in a fast fading channel is both analyzed and demonstrated via computer simulations.

2.3.1 Signal Detection in Slow Fading Channels

If the channel is slow fading, the ICI terms are not significant as described in [50] and

$$a_{i,l}[k, m] \approx 0 \quad \forall m \neq k. \quad (2.15)$$

As a result, the received signal (2.9) is expressed as a set of simultaneous equations

$$\mathbf{Y}[k] = \mathbf{A}[k, k]\mathbf{X}[k] + \mathbf{Z}[k], \quad k \in \mathcal{K} \quad (2.16)$$

where

$$\mathbf{A}[k, m] \triangleq \begin{bmatrix} a_{1,1}[k, m] & a_{2,1}[k, m] \\ a_{2,2}^*[k, m] & -a_{1,2}^*[k, m] \end{bmatrix} \text{ for } k, m \in \mathcal{K} \quad (2.17)$$

$$\mathbf{Y}[k] \triangleq [Y_1[k] \quad Y_2^*[k]]^T, \mathbf{X}[k] \triangleq [X_1[k] \quad X_2[k]]^T, \text{ and } \mathbf{Z}[k] \triangleq [Z_1[k] \quad Z_2^*[k]]^T.$$

Via the assumption that the channels do not change over an Alamouti codeword period, i.e., $a_{1,1}[k, k] = a_{1,2}[k, k] = \alpha_1[k]$ and $a_{2,1}[k, k] = a_{2,2}[k, k] = \alpha_2[k]$, space-time decoding is performed by multiplying both sides of (2.16) with $\mathbf{A}^H[k, k]$ to estimate the transmitted symbols $\tilde{\mathbf{X}}[k] = (|\alpha_1[k]|^2 + |\alpha_2[k]|^2)\mathbf{X}[k] + \mathbf{A}^H[k, k]\mathbf{W}[k]$. Note that the two symbols in $\tilde{\mathbf{X}}[k]$ are decoupled from each other. The final decisions are made independently $\hat{X}_i[k] = \arg \min_{X \in C_{QPSK}} \|\tilde{X}_i[k] - \rho[k]X\|, i \in \{1, 2\}$ with $\rho[k] \triangleq |\alpha_1[k]|^2 + |\alpha_2[k]|^2$.

2.3.2 Signal Detection in Fast Fading Channels

When the channel is fast fading, however, the approximation (2.15) is no longer valid and the received signal (2.9) is split into N_c equations as follows

$$\mathbf{Y}[k] = \mathbf{A}[k, k]\mathbf{X}[k] + \sum_{m \in \mathcal{K} \setminus k} \mathbf{A}[k, m]\mathbf{X}[m] + \mathbf{Z}[k], \quad k \in \mathcal{K}. \quad (2.18)$$

If I define $\tilde{\mathbf{A}}[k] \triangleq \begin{bmatrix} \alpha_1[k] & \alpha_2[k] \\ \alpha_2^*[k] & -\alpha_1^*[k] \end{bmatrix}$, where $\alpha_1[k] = a_{1,1}[k, k]$, $\alpha_2[k] = a_{2,1}[k, k]$, then $\tilde{\mathbf{A}}^H[k]\tilde{\mathbf{A}}[k] = \rho[k]\mathbf{I}_2$.

The following equation for each $k \in \mathcal{K}$ can be derived from (2.18), using the above identity

$$\tilde{\mathbf{Y}}[k] = \rho[k]\mathbf{X}[k] + \mathbf{C}_{INTRA}[k]\mathbf{X}[k] + \sum_{m \in \mathcal{K} \setminus k} \mathbf{C}_{INTER}[k, m]\mathbf{X}[m] + \tilde{\mathbf{Z}}[k] \quad (2.19)$$

where

$$\tilde{\mathbf{Y}}[k] \triangleq \tilde{\mathbf{A}}^H[k]\mathbf{Y}[k] \quad (2.20)$$

$$\mathbf{C}_{INTRA}[k] \triangleq \tilde{\mathbf{A}}^H[k]\mathbf{A}_\Delta[k] \quad (2.21)$$

$$\mathbf{C}_{INTER}[k, m] \triangleq \tilde{\mathbf{A}}^H[k] \mathbf{A}[k, m] \quad (2.22)$$

$$\tilde{\mathbf{Z}}[k] \triangleq \tilde{\mathbf{A}}^H[k] \mathbf{Z}[k] \quad (2.23)$$

$$\mathbf{A}_\Delta[k] \triangleq \mathbf{A}[k, k] - \tilde{\mathbf{A}}[k] \quad (2.24)$$

It can be observed that the second and the third terms on the right side of (2.19) show the effects of a time-variant channel. The second term shows the coupling effect between symbols in a codeword (intra-codeword coupling) and the third term shows the coupling effect between symbols in different codewords (inter-codeword coupling) or ICI. These two coupling effects create interference that lower the effective SNR at each subchannel, thereby degrading the performance.

To show the relative significance of the two coupling effects, the following two statistics and a coupling function are defined as,

$$\bar{C}_{INTRA} \triangleq \frac{1}{N_c} \sum_{k \in \mathcal{K}} E \left\{ \|\mathbf{C}_{INTRA}[k]\|^2 \right\} \quad (2.25)$$

$$\bar{C}_{INTER}[k_0] \triangleq \frac{1}{N_c} \sum_{k \in \mathcal{K}} E \left\{ \|\mathbf{C}_{INTER}[k, k + k_0]\|^2 \right\} \quad (2.26)$$

$$\Psi[k, k_0] \triangleq \begin{cases} \mathbf{C}_{INTRA}[k] & \text{if } k_0 = 0 \\ \mathbf{C}_{INTER}[k, k + k_0] & \text{otherwise.} \end{cases} \quad (2.27)$$

From (2.25), (2.26), and (2.27), the following statistic is obtained

$$\bar{\Psi}[k_0] \triangleq \frac{1}{N_c} \sum_{k \in \mathcal{K}} E \left\{ \|\Psi[k, k_0]\|^2 \right\} = \begin{cases} \bar{C}_{INTRA} & \text{if } k_0 = 0 \\ \bar{C}_{INTER}[k_0] & \text{otherwise.} \end{cases} \quad (2.28)$$

The statistic $\bar{\Psi}[0]$ shows the average intra-codeword coupling degree. When $k_0 \neq 0$, $\bar{\Psi}[k_0]$ is the average inter-codeword coupling amount from a subchannel which is k_0 times subcarrier spacing away from an observed subchannel.

2.3.3 Numerical Examples

In this section, the two coupling effects and performance degradation due to the coupling effects are demonstrated via simulation. A two transmit antenna and one receive antenna OFDM system is simulated. Exact channel estimation at the receiver is assumed. The bandwidth $B = 400kHz$, the FFT size $N = 128$, the CP length $D = 32$, the number of data carrying subchannels $N_c = 120$, consequently the number of virtual carriers is $N - N_c = 8$, and the OFDM symbol period $(N + D)T_s = 400\mu s$. Four subchannels on both ends of the spectrum are not used for data transmission. Each subcarrier is modulated by QPSK symbols. The performance criterion is the bit error rate (BER) versus SNR at the receiver. The total signal power from the two transmit antennas is used for the calculation of the SNR. The mobile channel used for simulation is a two path channel with equal power and delays of 0 and $4T_s$ respectively with each path experiencing independent Rayleigh fading. Jakes' model was used for the Rayleigh fading channel simulation [51]. Doppler frequency considered is $297Hz$ which results in more severe channel variation than the scenario in [38]. For the statistic (2.28) and the BER measurement, 1,000 OFDM symbols (500 Alamouti codewords) are transmitted and estimated.

Fig. 2.2 shows an empirical $\bar{\Psi}[k_0]/\bar{\Psi}[0]$, $k_0 \in \{0, \pm 1, \dots, \pm 10\}$ when $f_D = 297Hz$. The simulation result suggests that the intra-codeword coupling is much stronger than inter-codeword coupling. Fig. 2.3 displays BER vs. SNR for Doppler frequencies of 50 and $297Hz$, and shows the performance

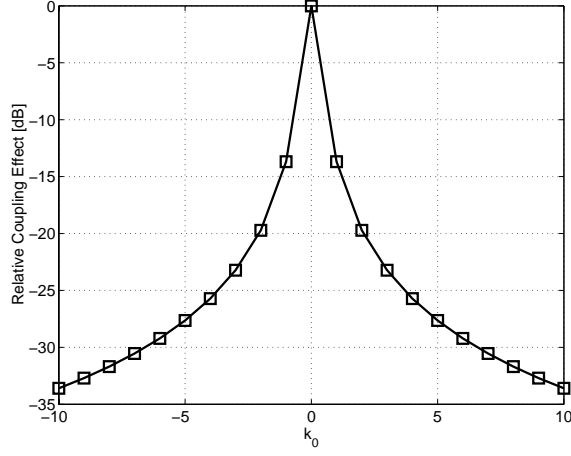


Figure 2.2: The relative significance of the two couplings caused by the time-variant channel, $10\log_{10}(\bar{\Psi}[k_0]/\bar{\Psi}[0])$ vs. k_0 , for $f_D = 297Hz$.

degradation in fast fading channels when the standard Alamouti decoding scheme is used. As the Doppler frequency increases from $50Hz$ to $297Hz$, the error performance is degraded significantly, especially for high SNR ($> 15dB$) channel environment. Given the relative significance of the two coupling effects in Fig. 2.2, it can be said that the performance degradation is mainly due to the intra-codeword coupling effect rather than the inter-codeword coupling effect. The performance degradation motivates a novel symbol estimation scheme which compensates for the coupling effects at a moderate complexity. In the next section, symbol estimation schemes are described that improve the performance under a fast fading channel environment.

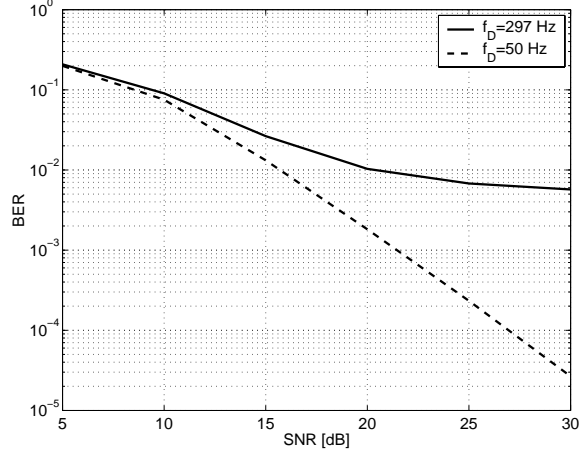


Figure 2.3: The BER performance vs. SNR of the Alamouti decoding scheme for $f_D=50$ and 297Hz.

2.4 Time Domain Block Linear Filter

Stamoulis *et. al.* proposed a TDBLF to mitigate the channel variation effect [38] where MIMO OFDM case was not described clearly. Therefore, I review the previous work briefly in this section. When two transmit antenna and one receive antenna are involved, a $2N \times 2N$ time domain block-linear filter is inserted right before the demodulating FFT, resulting in the following composite matrix

$$\overline{\mathbf{G}}_t \triangleq \mathbf{Q}^{(Rx)} \mathbf{W}_t \mathbf{H}. \quad (2.29)$$

The off-diagonal entries of $\overline{\mathbf{G}}_t$ are viewed as interference and the following signal to interference plus noise ratio $SINR_t(k)$ is defined

$$SINR_t(k) \triangleq \frac{E_x |\mathbf{e}_k^H \overline{\mathbf{G}}_t \mathbf{e}_k|^2}{\frac{\sigma_z^2}{2N} \text{tr}(\mathbf{W}_t \mathbf{W}_t^H) + E_x \sum_{m \neq k} |\mathbf{e}_k^H \overline{\mathbf{G}}_t \mathbf{e}_m|^2}. \quad (2.30)$$

I desire that the time domain block-linear filter maximizes the above $SINR_t(k)$, $k = 0, 1, \dots, 2N - 1$. It was shown [38] that an optimization problem can be formulated as

For each $k = 0, 1, \dots, 2N - 1$

$$\begin{aligned} \max_{\mathbf{w}_k} \mathbf{w}_k^H \mathbf{h}_k \mathbf{h}_k^H \mathbf{w}_k \\ \text{subject to } \mathbf{w}_k^H \left(\frac{\sigma_z^2}{E_x} \mathbf{I}_{2N} + \mathbf{R}_k \right) \mathbf{w}_k = 1 \end{aligned} \quad (2.31)$$

where $\mathbf{w}_k \triangleq \mathbf{W}_t^H \mathbf{q}_k$, $\mathbf{q}_k \triangleq \mathbf{Q}^{(Rx)} \mathbf{e}_k$, $\mathbf{h}_k \triangleq \mathbf{H} \mathbf{e}_k$, and $\mathbf{R}_k \triangleq \frac{\sigma_z^2}{E_s} \mathbf{I}_{2N} + \mathbf{H} \mathbf{H}^H - \mathbf{h}_k \mathbf{h}_k^H$. If no power control is adopted, the transmit power is equally divided, i.e., $\mathbf{E}[|X_i(k)|^2] = E_x$ for all i and k . The vector \mathbf{e}_k is the unit norm column vector of length $2N$ with the k -th entry of 1.

The above optimization problem is solved as

For each $k = 0, 1, \dots, 2N - 1$

$$\tilde{\mathbf{w}}_k = \mathbf{R}^{-1} \mathbf{h}_k \quad (2.32)$$

$$\mathbf{w}_{k,opt} = \tilde{\mathbf{w}}_k / |\tilde{\mathbf{w}}_k| \quad (2.33)$$

where $\mathbf{R} \triangleq \mathbf{H} \mathbf{H}^H + \frac{\sigma_z^2}{E_x} \mathbf{I}_{2N}$.

Note that only one matrix inversion is necessary in the filter design process. I also note that the normalization (2.33) is not required in the optimization process. The normalization is equivalent to scaling both the numerator and the denominator in (2.35). However, the normalization prevents overflow or underflow error that might happen in fixed point hardware/software implementation. From the above filter design procedure, I can obtain the following

$2N \times 2N$ time domain block-linear filter

$$\mathbf{W}_t = \mathbf{Q}^{(Rx)H} [\mathbf{w}_{0,opt} \quad \mathbf{w}_{1,opt} \quad \cdots \quad \mathbf{w}_{2N-1,opt}]^H. \quad (2.34)$$

Finally, transmitted signals are estimated using the above filter

$$\hat{X}(k) = \frac{[\mathbf{Q}^{(Rx)} \mathbf{W}_t \mathbf{Y}]_k}{\overline{G}_t(k, k)}, \quad k = 0, 1, \dots, 2N - 1 \quad (2.35)$$

where $\hat{X}(k)$ is the estimated symbol of $X(k)$. Note that the $(k + N)$ -th entry of \mathbf{X} is the k -th entry of \mathbf{X}_2 .

However, the filter design process and filtering process of the time domain block linear filter is computationally quite expensive. Detailed complexity evaluation will be done in Sec.5.4. Therefore, Chapters 3-5 propose computationally efficient signal detection methods.

Chapter 3

Decision Directed Receiver

This chapter proposes a decision directed receiver for OFDM systems with transmit diversity in fast fading channels [52][53]. The proposed decision directed receiver is based on the observation that when the normalized Doppler frequency is small, the inter-channel interfere (ICI) is from only a few nearest subchannels. Sec.3.1 proposes a decision directed receiver. Sec.3.2 demonstrate the error performance improvement by the proposed scheme.

3.1 Decision Directed Receiver

If the channels are time-variant over two symbol periods, however, the estimated symbols are expressed as

$$\begin{aligned}\tilde{\mathbf{X}}[k] &= \tilde{\mathbf{H}}^H[k]\tilde{\mathbf{H}}[k]\mathbf{X}[k] + \tilde{\mathbf{H}}^H[k]\mathbf{H}_\Delta[k]\mathbf{X}[k] \\ &\quad + \sum_{m \neq k} \tilde{\mathbf{H}}^H[k]\mathbf{A}[k, m]\mathbf{X}[m] + \tilde{\mathbf{H}}^H[k]\mathbf{Z}[k]\end{aligned}\quad (3.1)$$

where

$$\mathbf{H}_\Delta[k] \triangleq \begin{bmatrix} 0 & 0 \\ a_{2,2}^*[k] - a_{2,1}^*[k] & -a_{1,2}^*[k] + a_{1,1}^*[k] \end{bmatrix} \quad (3.2)$$

$$\mathbf{A}[k, m] \triangleq \begin{bmatrix} a_{1,1}[k, m] & a_{2,1}[k, m] \\ a_{2,2}^*[k, m] & -a_{1,2}^*[k, m] \end{bmatrix} \quad (3.3)$$

$$\tilde{\mathbf{H}}[k] \triangleq \begin{bmatrix} a_{1,1}[k] & a_{2,1}[k] \\ a_{2,1}^*[k] & -a_{1,1}^*[k] \end{bmatrix}. \quad (3.4)$$

When (3.1) is compared with (2.16), it can be observed that the second term on the right side of (3.1) shows the undesired component due to channel variation between consecutive OFDM symbols and the third term represents the ICI impairment. When the channel does not change over an Alamouti codeword period, $\tilde{\mathbf{H}}[k] = \mathbf{H}[k]$, $\mathbf{H}_\Delta[k] = \mathbf{0}_2$, and $\mathbf{A}[k, m] = \mathbf{0}_2$, $\forall m \neq k$, where $\mathbf{0}_2$ is 2×2 null matrix. Consequently, the two estimated signal expressions, (3.1) and (2.16) become identical. Thus when the channel is time-variant, the proposed approach improves the performance. With the time varying channel effect considered, the following decision directed technique is proposed.

Step#1) Initial Symbol Estimation

$$\tilde{\mathbf{X}}_{Init}[k] = \tilde{\mathbf{H}}^H[k] \mathbf{Y}[k] \quad (3.5)$$

Step#2) Intermediate Decisions

$$\hat{\mathbf{X}}[k] = Decision \left[\tilde{\mathbf{X}}_{Init}[k] \right] \quad (3.6)$$

Step#3) Estimated Symbol Update

$$\begin{aligned} \tilde{\mathbf{X}}[k] \leftarrow \tilde{\mathbf{X}}_{Init}[k] & - \tilde{\mathbf{H}}^H[k] (\mathbf{H}_\Delta[k] \hat{\mathbf{X}}[k] \\ & + \sum_{m=q, m \neq k}^{m+q} \mathbf{A}[k, m] \mathbf{X}[m]) \end{aligned} \quad (3.7)$$

Step#4) Final Decisions

$$\hat{\mathbf{X}}[k] = Decision \left[\tilde{\mathbf{X}}[k] \right] \quad (3.8)$$

If not satisfactory, go back to Step#3.

In step#3, I am using the result in [47] that ICI is due to only a few nearest adjacent subchannels ($2q$) when the Doppler frequency and the symbol period product is small (< 0.1).

3.2 Simulation Results

In this section, simulation experiments are conducted to demonstrate the efficacy of the proposed decoding scheme. A two transmit antenna and one receive antenna system with OFDM modulation is simulated. Exact channel estimation at the receiver is assumed. The entire bandwidth of $800kHz$ is divided into 128 subchannels. Four subchannels on each end are not used for data transmission. Each subcarrier is modulated by QPSK symbols. The guard interval is $40\mu s$. The performance criterion is bit error rate (BER) vs. signal-to-noise power ratio (SNR). The mobile channel used for simulation is a two path channel with equal power, each path experiencing independent Rayleigh fading. Considered Doppler frequencies are 50, 100, and $200Hz$. The total signal power from the two transmit antennas is used for the calculation of SNR. To measure the BER, 10,000 OFDM blocks are transmitted and estimated. The parameter $q = 1$ is used for the proposed decoding scheme. Iteration number $I = 1, 2$ are considered in the proposed scheme.

Fig.3.1-3.3 show the BER performance vs SNR for the Alamouti decoding scheme and the proposed decision directed decoding scheme when the

Doppler frequency is 50, 100, and 200 Hz in respect. As the Doppler frequency increases the BER performance of the Alamouti decoding scheme degrades severely because higher Doppler frequency means more rapid change of the channels. As can be observed in the figures, the proposed decision directed space-time decoding scheme improves the BER performance significantly for all considered Doppler frequencies. When the Doppler frequency is 200, 100, and 50 Hz , the proposed decision directed scheme improves the BER performance over a broad SNR range starting at 10, 15, and 20 dB , respectively. Note that more than one iteration for the proposed scheme does not improve the performance significantly, in that the decision directed ($I = 1$) curves are very close to the ($I = 2$) curves.

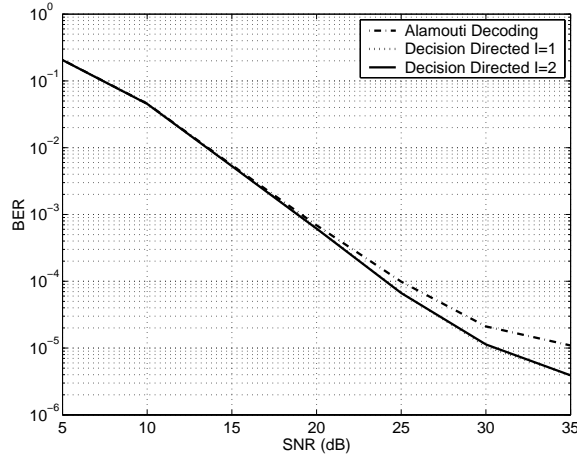


Figure 3.1: BER performance of the Alamouti decoding scheme and the proposed decision directed decoding scheme with $I = 1, 2$ when the Doppler frequency is 50 Hz .

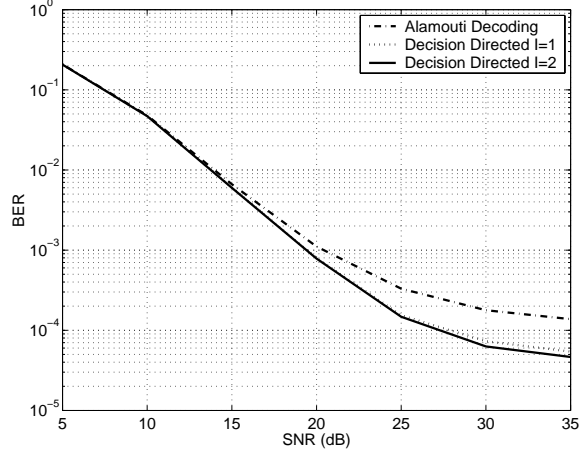


Figure 3.2: BER performance of the Alamouti decoding scheme and the proposed decision directed decoding scheme with $I = 1, 2$ when the Doppler frequency is $100Hz$.

3.3 Conclusions

In this chapter, an OFDM system with transmit diversity obtained using the Alamouti space-time code was considered. To better accommodate time-variant channels, a new decision directed space-time decoding scheme that extends the Alamouti decoding technique is proposed. Simulation experiments show that the proposed decision directed technique improves the BER performance with a moderate complexity increase when the channel is time-variant. However, the performance improvement is quite limited because the proposed receiver was developed under the assumption of correct intermediate decisions.

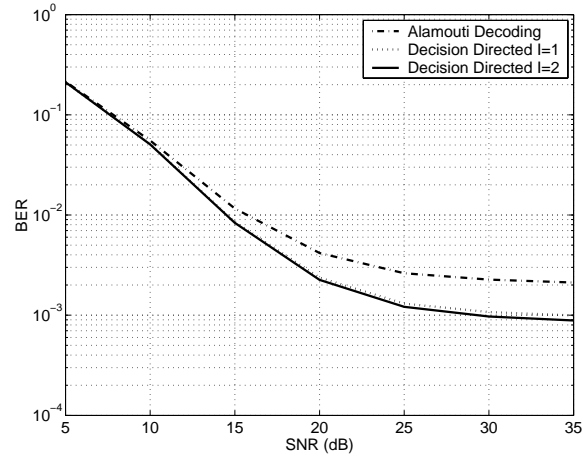


Figure 3.3: BER performance of the Alamouti decoding scheme and the proposed decision directed decoding scheme with $I = 1, 2$ when the Doppler frequency is $200Hz$.

Chapter 4

Sequence Estimation Receivers

In this chapter, sequence estimation receivers are proposed in the presence of the couplings discussed in Sec. 2.3.2 [54][55]. In Sec. 4.1, an MLSE approach is formulated for the system under consideration. In Sec. 4.2, an SDFSE with an AT is described as a suboptimal scheme reducing the complexity of the MLSE. Section 4.3 describes the AESE scheme. Section 4.4 considers the required computational complexity, especially comparing with the MMSE approach.

4.1 An MLSE Formulation

In this section, an MLSE scheme at the receiver is formulated. In this dissertation, the Alamouti coded OFDM system is considered while a trellis-based space time code was considered in previous work [34][35]. When the channel is fast fading, the two coupling effects described in section III.B need to be compensated. It was argued that if the normalized Doppler frequency is small, I can assume that ICI is from only a few nearest subchannels [47]. I argue that even when the normalized Doppler frequency is pretty large, I have only to consider ICI from a few nearest subchannels due to channel estimation

error as well as less significance of ICI from far away subchannels. By this assumption, the received signal (2.18) is simplified into

$$\begin{aligned} \mathbf{Y}[k] &= \mathbf{A}[k, k]\mathbf{X}[k] \\ &+ \sum_{m=\max(k-q, (N-N_c)/2), m \neq k}^{\min(k+q, (N+N_c)/2-1)} \mathbf{A}[k, m]\mathbf{X}[m] + \mathbf{Z}[k] \end{aligned} \quad (4.1)$$

where $2q$ is the number of subchannels considered as causing inter-codeword couplings.

It can be observed in (4.1) that the received signal is composed of the attenuated desired signal, ICI from $2q$ other subchannels, and additive noise.

Let

$$P\left(\mathbf{Y}_l, l \in \{1, 2\} \mid \mathbf{X}_i = \hat{\mathbf{X}}_i, i \in \{1, 2\}\right) \quad (4.2)$$

denote the conditional probability that $\mathbf{Y}_l, l \in \{1, 2\}$ are received under the assumption that the $\hat{\mathbf{X}}_i, i \in \{1, 2\}$ are transmitted. In the MLSE scheme, I estimate the transmitted sequence to be the sequence that maximizes the likelihood in (4.2). Since $\mathbf{W}[k]$ in (4.1) is a white complex Gaussian random process, I can show that the MLSE scheme amounts to computing [45]

$$(\hat{\mathbf{X}}[m] \mid m \in \mathcal{K}) = \arg \min_{(\hat{\mathbf{X}}[m] \mid m \in \mathcal{K})} \sum_{k \in \mathcal{K}} \xi_{MLSE}[k] \quad (4.3)$$

where

$$\xi_{MLSE}[k] = \left\| \mathbf{Y}[k] - \sum_{m=\max(k-q, (N-N_c)/2)}^{\min(k+q, (N+N_c)/2-1)} \mathbf{A}[k, m]\mathbf{X}[m] \right\|. \quad (4.4)$$

After a simple modification of the coupling function (2.27), the following function is defined

$$\Psi_{imp}[k, k_0] \triangleq \begin{cases} \rho[k]\mathbf{I}_2 + \Psi[k, k_0] & \text{if } k_0 = 0 \\ \Psi[k, k_0] & \text{if } k_0 \in \{\pm 1, \pm 2, \dots, \pm q\} \\ 0 & \text{else.} \end{cases} \quad (4.5)$$

If the above function is used, an equivalent metric to (4.4) can be written as

$$\xi_{MLSEq}[k] = \left\| \tilde{\mathbf{Y}}[k] - \sum_{m=\max(k-q, (N-N_c)/2)}^{\min(k+q, (N+N_c)/2-1)} \Psi_{imp}[k, m-k] \mathbf{X}[m] \right\|. \quad (4.6)$$

The function $\Psi_{imp}[k, m]$ can be considered as a sort of non-causal time-variant impulse response at time k with channel memory of $2q+1$, while $(\mathbf{X}[m] | m \in \mathcal{K})$ is the symbol sequence I need to detect. The state at k is defined as

$$\sigma_k \triangleq (\mathbf{X}[m] | m \in \{\max(k-q, (N-N_c)/2), \dots, \min(k+q, (N+N_c)/2-1)\}). \quad (4.7)$$

Dynamic programming based on the principle of optimality such as the Viterbi algorithm can simplify the minimization problem (4.3). The minimization problem under consideration, however, requires $Q^{2(2q)}$ MLSE states, where Q is the constellation size. Even for small Q , the minimization problem might be computationally prohibitive. In addition, merging is a random phenomenon and it is possible that no decision is made until the end of the entire sequence. Given that the length of the sequence $(\mathbf{X}[m] | m \in \mathcal{K})$ is N_c , this may result in an N_c codeword period delay [45].

The next section describes an SDFSE scheme with an AT which mitigates both the delay and the very high complexity problem of the MLSE.

4.2 An SDFSE Scheme with an AT

Among suboptimal but computationally feasible sequence estimation techniques is sequential sequence estimation. Sequential sequence estimation, which relieves the delay problem of the MLSE, can also be combined with decision feedback scheme to further reduce complexity [56]-[57]. By assuming that I have correctly recovered the sequence $\sigma_{k-} \triangleq (\hat{\mathbf{X}}[m] | m \in \{max(k - q, (N - N_c)/2), \dots, k - 1\})$ by the time I try to recover $\hat{\mathbf{X}}[k]$, an SDFSE scheme can be formulated as follows

$$\begin{aligned}
\text{For } k &= (N - N_c)/2 : (N + N_c)/2 - 1 & (4.8) \\
\hat{\sigma}_{k+} &= \arg \min_{\sigma_{k+}} \xi_{SDFSE}[k] \\
\hat{\mathbf{X}}[k] &\text{ is adopted and } \hat{\sigma}_{k+} \setminus \hat{\mathbf{X}}[k] \text{ is discarded} \\
k &\leftarrow k + 1
\end{aligned}$$

where

$$\begin{aligned}
\sigma_{k+} &\triangleq (\mathbf{X}[m] \in C_{QPSK} \times C_{QPSK} | \\
&m \in \{k, \dots, \min(k + q, (N + N_c)/2 - 1)\}) & (4.9)
\end{aligned}$$

$$\xi_{SDFSE}[k] \triangleq \left\| \check{\mathbf{Y}}[k] - \sum_{m=k}^{\min(k+q, (N+N_c)/2-1)} \mathbf{A}[k, m] \mathbf{X}[m] \right\|$$

$$\check{\mathbf{Y}}[k] \triangleq \mathbf{Y}[k] - \sum_{m=\max(k-q, (N-N_c)/2)}^{k-1} \mathbf{A}[k, m] \hat{\mathbf{X}}[m]. \quad (4.11)$$

Now the required number of metric calculations is $Q^{2(q+1)}$ for the estimation of symbols in a codeword.

Further complexity reduction via an AT: Now further complexity reduction is accomplished by using an AT. The idea of threshold, which is referred as the T-algorithm, was introduced to reduce the decoding complexity of the convolutional codes in [58], but no formula was proposed for selecting the threshold value. A similar idea was used in [46] in which posterior probabilities associated with one step previous states are calculated and a state is removed when the corresponding posterior probability is less than a threshold. Another method to set a threshold value was proposed in [59]. In [59], the threshold value is set so that the removal probability of a correct state is less than a target error probability. In this scheme, an instantaneous SNR is necessary to calculate the instantaneous threshold value though. The maximum possible threshold value can be used to avoid instantaneous threshold value calculation, which in turn decreases the efficiency of the threshold idea. On the other hand, in this dissertation, a threshold value is decided based on the time-variation degree of the channel without requiring the instantaneous SNR or posterior probability.

Under the assumption that a sequence σ_{k-} was recovered correctly, a simple metric is defined

$$\xi_{simple}[k] = \left\| \check{\mathbf{Y}}[k] - \mathbf{A}[k, k] \mathbf{X}[k] \right\|. \quad (4.12)$$

Comparison of (4.10) and (4.12) shows that the metric (4.10) involves a sequence σ_{k+} while the simple metric (4.12) considers only $\mathbf{X}[k]$. In other words, the metric (4.12) considers only the intra-codeword coupling effects while the metric (4.10) takes into account both coupling effects. From (4.10) and (4.12), the difference between the two metrics is bounded as follows

$$\forall \mathbf{X}[k] \in C_{QPSK} \times C_{QPSK} \text{ and } \sigma_{k+} \text{ with the } \mathbf{X}[k]$$

$$\begin{aligned} & \left| \xi_{simple}[k]_{\mathbf{X}[k]} - \xi_{SDFSE}[k]_{\sigma_{k+}} \right| \\ & \leq \left\| \sum_{m=k+1}^{\min(k+q, (N+N_c)/2-1)} \mathbf{A}[k, m] \hat{\mathbf{X}}[m] \right\| \\ & \leq \sqrt{2} \sum_{m=k+1}^{\min(k+q, (N+N_c)/2-1)} \|\mathbf{A}[k, m]\| \triangleq B[k] \end{aligned} \quad (4.14)$$

Note that the norm $\|\mathbf{X}\| = \sqrt{2}, \forall \mathbf{X} \in C_{QPSK} \times C_{QPSK}$ by assuming a constellation of unit amplitude symbols. I can observe that the bound $B[k]$ is a function of inter-codeword coupling.

Let $\mathbf{X}_{subopt}[k]$ be the minimizer of the metric (4.12), then

$$\begin{aligned} & \left| \xi_{simple}[k]_{\mathbf{X}_{subopt}[k]} - \xi_{simple}[k]_{\mathbf{X}[k]} \right| \\ & \leq \left\| \mathbf{A}[k, k] (\mathbf{X}_{subopt}[k] - \mathbf{X}[k]) \right\| \\ & \leq \left\| \mathbf{A}[k, k] \right\| \left\| \mathbf{X}_{subopt}[k] - \mathbf{X}[k] \right\| \triangleq C[k]. \end{aligned} \quad (4.15)$$

The bound $C[k]$ is a function of the intra-codeword coupling effect.

The following relationship between the above two bounds can be induced from Fig. 2.2

$$E\{C[k]\} = \frac{2 + \sqrt{2}}{2} \cdot E\{\|\mathbf{A}[k, k]\|\} > 2E\{B[k]\}. \quad (4.16)$$

The above inequality again implies the following relation

$$\begin{aligned} \mathcal{S}_k \subset \{ \mathbf{X}[k] \in C_{QPSK} \times C_{QPSK} \mid \\ \left| \xi_{simple}[k]_{\mathbf{X}_{subopt}[k]} - \xi_{simple}[k]_{\mathbf{X}[k]} \right| \leq C[k] \} \end{aligned} \quad (4.17)$$

where

$$\begin{aligned} \mathcal{S}_k \triangleq \{ \mathbf{X}[k] \in C_{QPSK} \times C_{QPSK} \mid \\ \left| \xi_{simple}[k]_{\mathbf{X}_{subopt}[k]} - \xi_{simple}[k]_{\mathbf{X}[k]} \right| \leq 2B[k] \}. \end{aligned} \quad (4.18)$$

Meanwhile, if I let $\mathbf{X}_{opt}[k]$ be the minimizer of the metric (4.10), the relationship between the two minimizers is derived from (4.14)

$$\left| \xi_{simple}[k]_{\mathbf{X}_{subopt}[k]} - \xi[k]_{simple} \big|_{\mathbf{X}_{opt}[k]} \right| \leq 2B[k] \quad (4.19)$$

which implies that $\mathbf{X}_{opt}[k] \in \mathcal{S}_k$.

A small set of probable minimizers of the metric (4.10) can be chosen via the simple metric (4.12). This is where the idea of the adaptive threshold (AT) method is used. The smaller the bound $B[k]$ compared to $C[k]$, the smaller $|\mathcal{S}_k|$ becomes, where $|\mathcal{S}_k|$ is defined as the number of elements in \mathcal{S}_k . The set \mathcal{S}_k can be regarded as a candidate set of $\mathbf{X}[k]$. After the selection of candidates of $\mathbf{X}[k]$ which requires Q^2 metric calculations of $\xi_{simple}[k]$, $|\mathcal{S}_k| \cdot Q^{2q}$

metric calculations are necessary to find the minimizer of $\xi_{SDFSE}[k]$. In other words, intra-codeword coupling effects are first considered for the estimation of the transmitted symbols and the inter-codeword coupling effects are considered only when there are more than one contender. Note that when large q needs to be considered, the idea of a threshold can be further exploited by defining another simple metric including a few inter-codeword coupling effects. I also note that the AT decreases not only the number of metric calculations but also the complexity of each metric calculation via (4.12).

4.3 An AESE Scheme

To further reduce the average complexity of the SDFSE scheme with an AT, an AESE is proposed in this section. The basic idea is that when the instantaneous channel variation is small, thus $\|\mathbf{C}_{INTRA}[k]\|$ for each $k \in \mathcal{K}$ is smaller than a threshold (T_{AESE}), the simple Alamouti decoding scheme is used. On the other hand, the SDFSE scheme with an AT is used to mitigate the performance degradation when the instantaneous channel variation is large and consequently $\|\mathbf{C}_{INTRA}[k]\|$ is larger than the threshold. Fig. 4.1 is a block diagram of the proposed adaptive effort receiver. This scheme is based on the observation that high Doppler frequency implies a statistical fast fading channel but it does not necessarily mean significant instantaneous channel variation. To quantify the effectiveness of the proposed AESE, I define the following probability that an instantaneous channel variation is significant and, consequently, an Alamouti codeword is estimated via the SDFSE scheme with

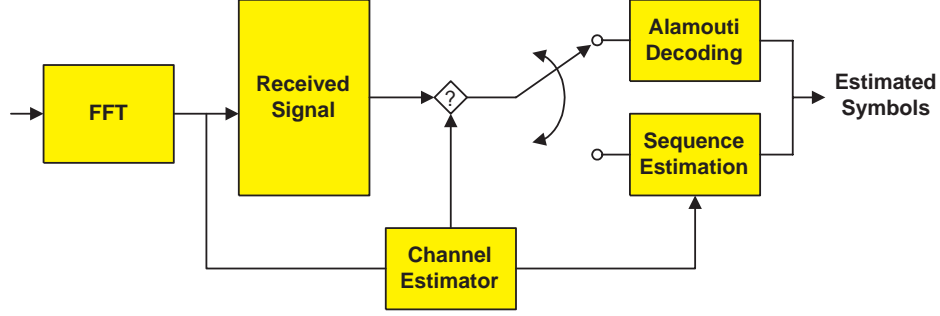


Figure 4.1: Block diagram of the proposed adaptive effort receiver. When the instantaneous channel time-variation is significant the SDFSE with AT is used, and when it is not significant the simple Alamouti decoding is used.

an AT

$$P_{AESE} \triangleq P \left(\| \mathbf{C}_{INTRA}[k, k] \| > T_{AESE} \right). \quad (4.20)$$

The trade off between complexity and performance can be made via T_{AESE} in the AESE scheme. Larger T_{AESE} means that more symbols are estimated via the simple Alamouti decoding. Thus complexity can be reduced by using larger T_{AESE} but the performance will be degraded at the same time.

4.4 Computational Complexity

In this subsection, the computational complexity of various schemes is compared. The required number of metric calculations for the proposed schemes are summarized in Table 4.1. Since I am considering $q = 1$, the number of metric calculations required in SDFSE with an AT is $(1 + \overline{|\mathcal{S}_k|})Q^2$, where

$\overline{|\mathcal{S}_k|} = \sum_{i=2}^{Q^2} i \cdot \text{Prob}(|\mathcal{S}_k| = i)$. In the process of decoding N_c Alamouti codewords, $N_c(1 + \overline{|\mathcal{S}_k|})Q^2 \cdot 4$ multiplications are required per Alamouti codeword period. The average complexity can be further reduced via the adaptive effort scheme with only negligible performance degradation.

To assess the complexity of the time domain MMSE filter approach, the MMSE filter design procedure as well as the filtering procedure needs to be included. In the filter design procedure, the correlation matrix (\mathbf{R}_{yy} in Sec.IV.B in [38]) is constructed first, whose size is $2N \times 2N$ for the two transmit and one receive antenna systems, requiring $(2N)^3$ multiplications (Using the sparse structure of the corresponding matrices, complexity is lowered to $(2N)^2 \times (2L)$, where L is the number of multipaths for each channel). Then the inverse of the correlation matrix is calculated which requires $(2N)^3$ multiplications. Finally, time variant filter is designed as described in Sec.IV.B ($(2N)^3$ multiplications). In the filtering process, $(2N)^2$ multiplications are required since the length of the filter is $2N$. Therefore, roughly $3 \times (2N)^3 + (2N)^2$ multiplications are required per Alamouti codeword period. The low rank approximation of the correlation matrix that was used in [60] can be adopted to reduce complexity in the filter design process. Unlike in [60], however, a low rank approximation is necessary per codeword period. It seems that the computationally expensive singular value decomposition (SVD) in the approximation process does not reduce the complexity dramatically.

Since I am considering parameters $N = 128$ and $Q = 4$, the complexity of the proposed SDFSE with an AT is much lower than the MMSE approach.

Table 4.1: Required number of metric calculations for an Alamouti codeword estimation in various symbol estimation schemes.

Decoding Scheme	Required number of metric calculations
Alamouti Decoding Scheme	$2 \cdot Q$
SDFSE	$Q^{2(q+1)}$
SDFSE with an AT	$Q^2 + \mathcal{S}_k Q^{2q}$
AESE	$P_{AESE}(Q^2 + \mathcal{S}_k \cdot Q^{2q}) + (1 - P_{AESE})2Q$

Since the MMSE scheme complexity does not depend on the constellation size Q , the relative complexity of the proposed schemes grows as larger constellations are used. But under the harsh channel environment I am considering here, the small signal constellation may be used to achieve a proper error performance.

4.5 Simulation Results

In this section, the error performance and complexity of the following schemes are compared via simulation, the Alamouti decoding scheme, the SDFSE scheme with an AT, the AESE scheme, the differential STBC scheme, and the MMSE filter approach. The simulation scenario is the same as in Sec. 2.3.3. I consider only the higher Doppler frequency of $297Hz$, resulting in a normalized Doppler frequency of $f_D(N + D)T_s = 0.12$. Unlike in Sec. 2.3.3, I consider both cases with and without ideal CSI at the receiver. Considered values for T_{AESE} in the AESE scheme are 0.3 and 0.4. Exact noise power is assumed to be available for the MMSE approach.

Fig. 4.2 shows the BER performance vs. SNR of the various decoding schemes when the ideal CSI is assumed. The time domain MMSE filter approach shows the best performance. The performance of the proposed SDFSE with an AT falls between the Alamouti performance and that of the MMSE approach. It can be observed that as the parameter q increases in the proposed SDFSE with an AT, the performance approaches that of the MMSE filter. For the SNR range from 5 to 25dB, the proposed SDFSE with an AT ($q = 2$) shows almost the same performance as that of MMSE. When the SNR is as high as 30dB, there exists a performance difference though. The performance gap seems to be due to the fact that the MMSE approach considers inter-codeword coupling from all subchannels while the SDFSE with an AT considers inter-codeword coupling from only $2q$ adjacent subchannels. The performance gap suggests that, as the SNR gets higher, more subchannels need to be considered from which inter-codeword coupling is caused.

Fig. 4.3 shows the BER performance when the CSI is estimated via the channel estimation technique in [38]. The performance degradation due to channel estimation error can be observed. The decoding schemes react differently to the channel estimation error. The error performance of the Alamouti decoding and the SDFSE with an AT ($q = 0$) is almost identical as when the ideal CSI is assumed. With channel estimation error, however, the SDFSE with an AT ($q = 2$) shows almost the same performance as that of the SDFSE with an AT ($q = 1$), which suggests that inter-codeword coupling $\mathbf{A}[k, k+2]$ is more susceptible to CSI estimation error than $\mathbf{A}[k, k]$ and $\mathbf{A}[k, k+1]$ are. The

MMSE approach shows the most significant performance gap between ideal and estimated CSI. The BER performance in Fig.5.4 suggests that with CSI estimation error, large q does not have to be adopted in the SDFSE with an AT. It shows also that with CSI estimated, the proposed SDFSE with an AT ($q = 1$) shows negligible performance degradation compared to the MMSE approach.

Fig. 4.3 also shows the performance of the differential scheme [44]. Although the differential scheme eliminates the need for CSI estimation which is more beneficial when the channels change very fast, its performance loss due to the non-quasi-static channels is much more severe than the performance loss of other coherent schemes due to CSI estimation error. It seems that the performance loss is caused by the strict assumption of the differential scheme that the channels do not change over two Alamouti codeword periods, i.e., four OFDM symbol periods. Note that the Alamouti decoding scheme assumes that the channels do not change over only two OFDM symbol periods.

Fig. 4.4 shows the probability of the number of candidates in the SDFSE with an AT ($q = 1$). It can be observed that more candidates are selected when the SNR is low. This is because that more constellation points satisfy the constraint (4.18) due to dominant background noise. As the SNR increases, the number of candidates significantly decreases. When the SNR is $20dB$, only one candidate is selected with probability of 0.9. The corresponding $\overline{|\mathcal{S}_k|} = 0.2$, hence, the complexity of the SDFSE with an AT is $N_c \times 1.2 \times Q^2 \times 4$ multiplications per Alamouti codeword period. The complexity of

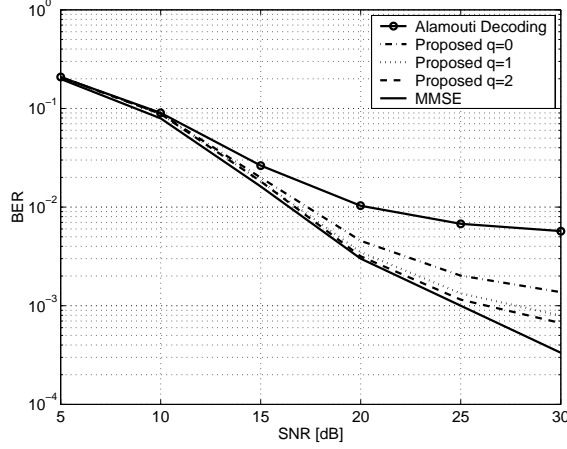


Figure 4.2: BER performance (perfect CSI) of the Alamouti Decoding, proposed SDFSE with an AT($q = 0, 1, 2$), the Time Domain MMSE.

the proposed approach is much lower than $3 \times (2N)^3 + (2N)^2$ of the MMSE approach when a moderate Q is assumed. The complexity ratio of the proposed receiver to the MMSE approach is approximately $\frac{5Q^2}{24N^2}$.

Fig. 4.5 shows a coded BER performance (CSI is estimated) of the Alamouti decoding, proposed SDFSE with an AT ($q=1,2$), and the previous TDBLF. The 1/2 rate convolutional coding and corresponding Viterbi decoding (constraint length of 3, storage depth of 64) is used in conjunction with bit level interleaving. Comparing Fig. 4.3 and 4.5, significant coding gain of all the decoding methods can be observed. At the target BER of 10^{-3} , the coding gain of the proposed SDFSE with an AT is as big as $12dB$. It can be observed that the relative performance of the various decoding schemes stays almost the same as in Fig. 4.3.

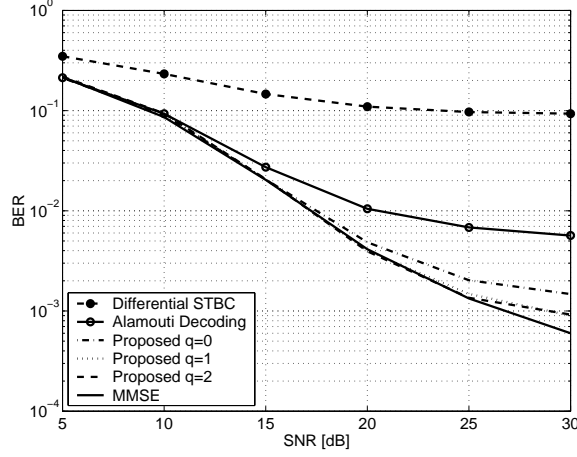


Figure 4.3: BER performance (estimated CSI) of the Alamouti Decoding, proposed SDFSE with an AT($q = 0, 1, 2$), the Time Domain MMSE, and differential STBC (no CSI estimation is necessary).

Fig.4.6 compares the performance of SDFSE with an AT ($q = 1$), AESE with $T_{AESE} = 0.3$ and 0.4 , and the MMSE filter approach. As can be seen in the figure, AESE scheme shows negligible performance degradation compared to SDFSE with an AT ($q = 1$) when the threshold value T_{AESE} is 0.3 . The probability $P_{AESE} = 58\%$ when $T_{AESE} = 0.3$. Therefore, about 42% of transmitted signals are estimated via the Alamouti decoding scheme even when the Doppler frequency is as high as $297Hz$ if $T_{AESE} = 0.3$. Although higher T_{AESE} can be used to further decrease the complexity (When $T_{AESE} = 0.4$, the probability goes down to 35% .), there exist significant performance gap. Therefore, it can be concluded that the proposed AESE with an appropriate T_{AESE} is an attractive receiver for Alamouti coded OFDM systems in fast

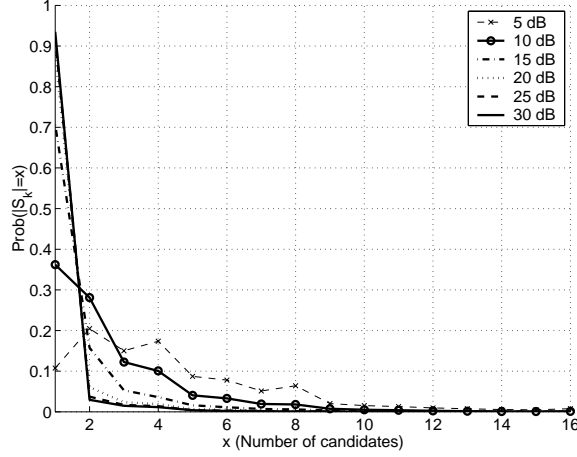


Figure 4.4: Number of candidates in the proposed SDFSE with an AT ($q = 1$) for various SNR values. Estimated CSI is used.

fading channels.

4.6 Conclusions

In Alamouti coded OFDM systems, the time variation of a channel causes both inter-codeword and intra-codeword couplings, which significantly degrade the performance of Alamouti decoding. It was shown that the performance degradation can be mitigated by the SDFSE scheme with an AT at a much lower complexity (when compared with the previous MMSE approach and a small constellation is assumed), exploiting the relative significance of the two couplings. It was also shown that the performance difference between the MMSE and the SDFSE with an AT becomes smaller when CSI estimation error is taken into account. When a very large constellation and a small FFT

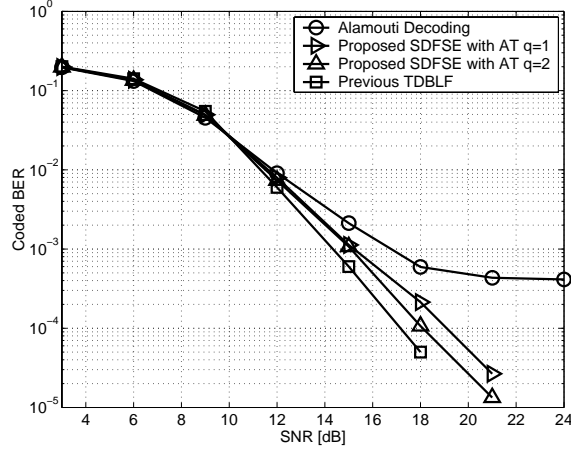


Figure 4.5: Coded BER performance (estimated CSI) of the Alamouti Decoding, proposed SDFSE with an AT($q = 1, 2$), and the Time Domain MMSE. Convolutional coding of rate $1/2$ is used in conjunction with a bit level interleaving.

size are adopted, however, the SDFSE with an AT may require higher complexity than the MMSE approach, making it not a preferred choice. A further reduction in average complexity was achieved based on the observation that high Doppler frequency does not necessarily mean significant instantaneous channel variation all the time, which motivated the development of the adaptive effort receiver. Simulation experiment demonstrated the efficacy of the proposed SDFSE with an AT and AESE schemes.

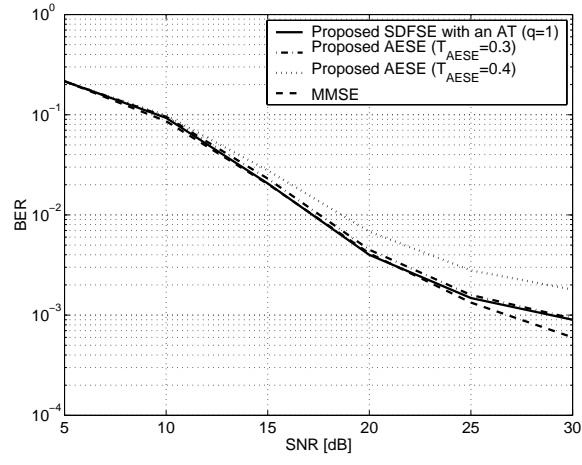


Figure 4.6: BER performance (estimated CSI) of AESE with $T_{AESE}=0.3$ and 0.4, SDFSE with an AT($q = 1$), the time domain MMSE.

Chapter 5

Frequency Domain Block Linear Filter

Chapter 4 proposed sequence estimation receivers that show a good trade off between complexity and error performance, compared to the previous TDBLF. The drawbacks of the sequence estimation, however, are that the complexity is time-variant which is not amenable to hardware implementations and that the complexity depends on the constellation size. In this chapter, I propose a frequency domain block-linear filter (FDBLF) whose size $2N \times (4q + 2)$ is much smaller than the time domain filter in Sec.2.4 [61]. The complexity of the proposed FDBLF is both time-invariant and independent of the constellation size. First, Sec.5.1 extends a previous block diagonal approximation of single input single output (SISO) system to MIMO case. Based on the extended block diagonal approximation, Sec.5.2 proposes a FDBLF. Finally, Sec.5.3 considers receiver combining for more than one receive antenna systems.

5.1 Block Diagonal Approximation

I investigate the structure of \mathbf{G} defined as

$$\mathbf{G} \triangleq \begin{bmatrix} \mathbf{G}_{11} & \mathbf{G}_{21} \\ \mathbf{G}_{22} & \mathbf{G}_{12} \end{bmatrix} \triangleq \begin{bmatrix} \mathbf{Q}H_{11}\mathbf{Q}^H & \mathbf{Q}H_{21}\mathbf{Q}^H \\ \mathbf{Q}^H H_{22}^* \mathbf{Q} & -\mathbf{Q}^H H_{12}^* \mathbf{Q} \end{bmatrix} = \mathbf{Q}^{(Rx)} \mathbf{H}. \quad (5.1)$$

Note that \mathbf{G}_{il} , $i, l = 1, 2$ denotes the subsystem reflecting the channel between the i -th transmit antenna and the receive antenna during the l -th symbol period. Instead of analyzing all the entries of \mathbf{G} , I investigate the submatrix \mathbf{G}_{11} . The (k, m) -th entry of \mathbf{G}_{11} is expressed as

$$G_{11}(k, m) = \frac{1}{\sqrt{N}} \sum_{p=0}^{L-1} \mathcal{H}_p(k, m) e^{-j2\pi kp/N} \quad (5.2)$$

where

$$\mathcal{H}_p(k, m) \triangleq \frac{1}{\sqrt{N}} \sum_{n=0}^{N-1} h_{1,1}(n, p) e^{-j2\pi n(k-m)/N}. \quad (5.3)$$

From (5.2), I can derive an upper bound of $|G_{11}(k, m)|$ as

$$|G_{11}(k, m)| \leq \frac{1}{\sqrt{N}} \sum_{p=0}^{L-1} |\mathcal{H}_p(k, m) e^{-j2\pi kp/N}| \quad (5.4)$$

$$= \frac{1}{\sqrt{N}} \sum_{p=0}^{L-1} |\mathcal{H}_p(k, m)| \quad (5.5)$$

Note that $\mathcal{H}_p(k, m)$ is the $(k - m)$ -th harmonic frequency coefficient of the time-variant p -th multipath. It was shown that when the channel variation is not severe, each path can be assumed to change in a linear fashion in [47]. If a multipath changes in a linear fashion, $|\mathcal{H}_p(k, m)|$ decreases dramatically as $|k - m|$ increases. I also showed that even when the channel variation is rather severe, inter-carrier interference (ICI) from far away subchannels may be ignored because of channel estimation error as well as its less significance in magnitude [55]. Therefore, each submatrix of \mathbf{G} can be approximated as a

band matrix with both lower and upper bandwidth of q [62], i.e.,

$$|G_{il}(k, m)| \approx 0 \text{ if } |k - m| > q, \quad 1 \leq i, l \leq 2. \quad (5.6)$$

Using (5.6), I perform a block diagonal approximation that is illustrated for $q = 1$ in Fig.5.1. Fig.5.1 shows that submatrices are approximately band matrices. The dimension of the original matrix is $2N \times 2N$ and that of the block diagonal approximated matrix is $(4q + 2)(N - 2q) \times (4q + 2)(N - 2q)$. I can observe that some significant terms are ignored in the approximation process. A general block diagonal approximation can be expressed as

$$\mathcal{Y} \approx \mathcal{G}\mathcal{X} + \mathcal{Z} \quad (5.7)$$

$$\begin{aligned} \text{where } \mathcal{Y} &\triangleq [\mathbf{Y}_{1,q}^T \quad \mathbf{Y}_{2,q}^H \quad \mathbf{Y}_{1,q+1}^T \quad \mathbf{Y}_{2,q+1}^H \quad \cdots \quad \mathbf{Y}_{1,N-1-q}^T \quad \mathbf{Y}_{2,N-1-q}^H]^T \\ \mathcal{X} &\triangleq [\mathbf{X}_{1,q}^T \quad \mathbf{X}_{2,q}^T \quad \mathbf{X}_{1,q+1}^T \quad \mathbf{X}_{2,q+1}^T \quad \cdots \quad \mathbf{X}_{1,N-1-q}^T \quad \mathbf{X}_{2,N-1-q}^T]^T \\ \mathcal{Z} &\triangleq [\mathbf{Z}_{1,q}^T \quad \mathbf{Z}_{2,q}^H \quad \mathbf{Z}_{1,q+1}^T \quad \mathbf{Z}_{2,q+1}^H \quad \cdots \quad \mathbf{Z}_{1,N-1-q}^T \quad \mathbf{Z}_{2,N-1-q}^H]^T \\ \mathbf{Y}_{l,k} &\triangleq [Y_l(k-q) \quad \cdots \quad Y_l(k) \quad \cdots \quad Y_l(k+q)]^T \\ \mathbf{X}_{i,k} &\triangleq [X_i(k-q) \quad \cdots \quad X_i(k) \quad \cdots \quad X_i(k+q)]^T \\ \mathbf{Z}_{l,k} &\triangleq [Z_l(k-q) \quad \cdots \quad Z_l(k) \quad \cdots \quad Z_l(k+q)]^T \\ \mathcal{G} &\triangleq \text{Diag}(\mathcal{G}_q, \mathcal{G}_{q+1}, \cdots, \mathcal{G}_{N-1-q}) \\ \mathcal{G}_k &\triangleq \begin{bmatrix} \mathbf{G}_{11,k} & \mathbf{G}_{21,k} \\ \mathbf{G}_{22,k} & \mathbf{G}_{12,k} \end{bmatrix}. \end{aligned}$$

The entries of the matrix $\mathcal{G}_k \in \mathbb{C}^{(4q+2) \times (4q+2)}$ is

$$\begin{aligned} G_{il,k}(m, n) &\triangleq \begin{cases} G_{il}(k-q+m, k-q+n) & \text{if } |k-m| \leq q \\ 0 & \text{otherwise,} \end{cases} \\ &, 0 \leq m, n \leq 2q, \quad i, l = 1, 2. \end{aligned} \quad (5.8)$$

Once the block diagonal approximation is done, I can divide the large equation (5.7) into the following small equations for each $k = q, q+1, \dots, N-q$

$$\mathbf{y}_k \approx \mathcal{G}_k \mathbf{x}_k + \mathbf{z}_k \quad (5.9)$$

where $\mathbf{x}_k \triangleq [\mathbf{X}_{1,k}^T \quad \mathbf{X}_{2,k}^T]^T$, $\mathbf{y}_k \triangleq [\mathbf{Y}_{1,k}^T \quad \mathbf{Y}_{2,k}^H]^T$, $\mathbf{z}_k \triangleq [\mathbf{Z}_{1,k}^T \quad \mathbf{Z}_{2,k}^H]^T$.

Numerical Example: To present the feasibility of the block diagonal approximation, I provide a numerical example of the sparse structure of the system matrix. Fig.5.2 is an instantaneous magnitude of entries of the system matrix. The FFT size used is 128. A spectral bandwidth of 400 kHz is assumed. Doppler frequency is 297 Hz which leads to the normalized Doppler frequency of 0.1188 ($f_D(N + \nu)T_s$). Equal gain two path channels with delays of 0 and $4T_s$ are simulated. As can be observed in Fig.5.2, the submatrices in (5.1) are close to band matrices. The off diagonal terms become smaller as the entry position is further from the diagonal. I can also observe the frequency selectivity of the channels.

5.2 Frequency Domain Block Linear Filter

In this section, a frequency domain block linear filter (FDBLF) is proposed exploiting the block diagonal approximation in the previous subsection.

In the process of the block diagonal approximation, I ignored not only the negligible terms $G_{ii}(k, m)$ with $|k - m| > q$ but also some significant terms $G_{ii}(k, m)$ with $|k - m| \leq q$. If I use the example when $q = 1$, a more exact small equation when $k = 2$ is expressed as

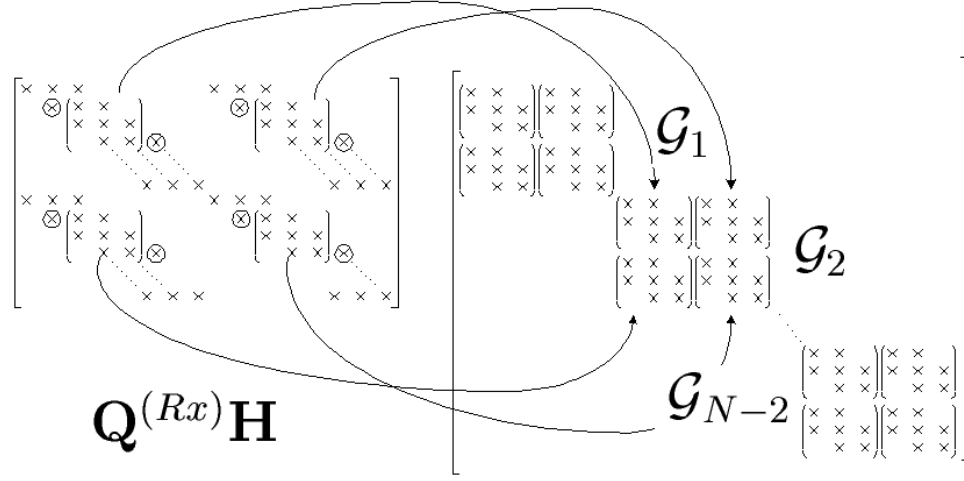


Figure 5.1: Illustration of a block diagonal approximation when $q = 1$. The entries that are significant but are approximated as 0 in the block diagonal approximation are denoted as circled crosses.

$$\mathcal{Y}_2 = \mathcal{G}_2 \mathcal{X}_2 + \mathcal{G}_2^{upper} \mathcal{X}_1 + \mathcal{G}_2^{lower} \mathcal{X}_3 + \mathcal{Z}_2 \quad (5.10)$$

where

$$\mathcal{G}_2 = \begin{bmatrix} \mathbf{G}_{11,2} & \mathbf{G}_{21,2} \\ \mathbf{G}_{22,2} & \mathbf{G}_{12,2} \end{bmatrix} \quad (5.11)$$

$$\mathcal{G}_2^{upper} = \begin{bmatrix} G_{11}(1,0) & \mathbf{0}_{1 \times 2} & G_{21}(1,0) & \mathbf{0}_{1 \times 2} \\ \mathbf{0}_{2 \times 1} & \mathbf{0}_{2 \times 2} & \mathbf{0}_{2 \times 1} & \mathbf{0}_{2 \times 2} \\ G_{22}(1,0) & \mathbf{0}_{1 \times 2}^T & G_{12}(1,0) & \mathbf{0}_{1 \times 2} \\ \mathbf{0}_{2 \times 1} & \mathbf{0}_{2 \times 2} & \mathbf{0}_{2 \times 1} & \mathbf{0}_{2 \times 2} \end{bmatrix} \quad (5.12)$$

$$\mathcal{G}_2^{lower} = \begin{bmatrix} \mathbf{0}_{2 \times 2} & \mathbf{0}_{2 \times 1} & \mathbf{0}_{2 \times 2} & \mathbf{0}_{2 \times 1} \\ \mathbf{0}_{1 \times 2} & G_{11}(3,4) & \mathbf{0}_{1 \times 2} & G_{12}(3,4) \\ \mathbf{0}_{2 \times 2} & \mathbf{0}_{2 \times 1} & \mathbf{0}_{2 \times 2} & \mathbf{0}_{2 \times 1} \\ \mathbf{0}_{1 \times 2}^T & G_{22}(3,4) & \mathbf{0}_{1 \times 2} & G_{12}(3,4) \end{bmatrix}. \quad (5.13)$$

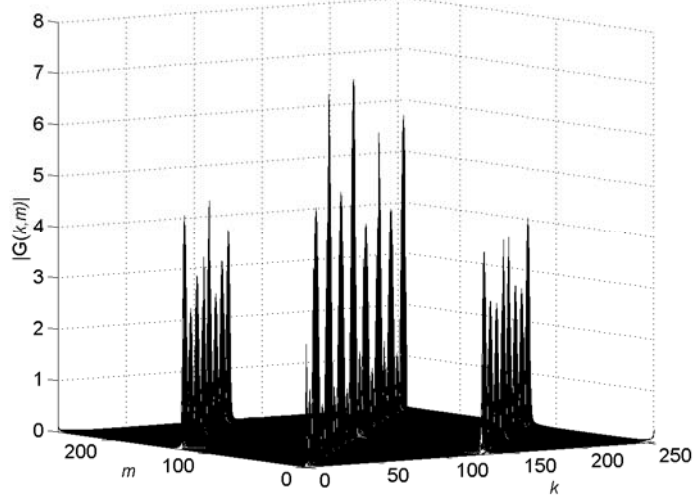


Figure 5.2: An Example of $|G(k, m)|$, $0 \leq k, m \leq 2N - 1$.

The first term on the right side of (5.10) is regarded as desired component, the second and the third terms are considered as interference.

The exact expression is generalized for an arbitrary q and k as

$$\mathcal{Y}_k = \mathcal{G}_k \mathcal{X}_k + \mathcal{G}_k^{upper} \mathcal{X}_{k-q} + \mathcal{G}_2^{lower} \mathcal{X}_{k+q} + \mathcal{Z}_k \quad (5.14)$$

where

$$\mathcal{G}_k^{upper} \triangleq \begin{bmatrix} \mathbf{G}_{11,k}^{upper} & \mathbf{0}_{q \times (q+1)} & \mathbf{G}_{21,k}^{upper} & \mathbf{0}_{q \times (q+1)} \\ \mathbf{0}_{(q+1) \times q} & \mathbf{0}_{(q+1) \times (q+1)} & \mathbf{0}_{(q+1) \times q} & \mathbf{0}_{(q+1) \times (q+1)} \\ \mathbf{G}_{22,k}^{upper} & \mathbf{0}_{q \times (q+1)} & \mathbf{G}_{12,k}^{upper} & \mathbf{0}_{q \times (q+1)} \\ \mathbf{0}_{(q+1) \times q} & \mathbf{0}_{(q+1) \times (q+1)} & \mathbf{0}_{(q+1) \times q} & \mathbf{0}_{(q+1) \times (q+1)} \end{bmatrix} \quad (5.15)$$

$$\mathcal{G}_k^{lower} \triangleq \begin{bmatrix} \mathbf{0}_{(q+1) \times (q+1)} & \mathbf{0}_{(q+1) \times q} & \mathbf{0}_{(q+1) \times (q+1)} & \mathbf{0}_{(q+1) \times q} \\ \mathbf{0}_{q \times (q+1)} & \mathbf{G}_{11,k}^{lower} & \mathbf{0}_{q \times (q+1)} & \mathbf{G}_{21,k}^{lower} \\ \mathbf{0}_{(q+1) \times (q+1)} & \mathbf{0}_{(q+1) \times q} & \mathbf{0}_{(q+1) \times (q+1)} & \mathbf{0}_{(q+1) \times q} \\ \mathbf{0}_{q \times (q+1)} & \mathbf{G}_{22,k}^{lower} & \mathbf{0}_{q \times (q+1)} & \mathbf{G}_{12,k}^{lower} \end{bmatrix} \quad (5.16)$$

$$\mathbf{G}_{il,k}^{upper} \triangleq \begin{bmatrix} G_{il}(k-q, k-2q) & \cdots & G_{il}(k-q, k-q-1) \\ 0 & \cdots & G_{il}(k-q+1, k-q-1) \\ \vdots & \ddots & \vdots \\ 0 & \cdots & G_{il}(k-1, k-q-1) \end{bmatrix} \quad (5.17)$$

$$\mathbf{G}_{il,k}^{lower} \triangleq \begin{bmatrix} G_{il}(k+1, k+q+1) & \cdots & 0 \\ G_{il}(k+2, k+q+1) & \cdots & 0 \\ \vdots & \ddots & \vdots \\ G_{il}(k+q, k+q+1) & \cdots & G_{il}(k+q, k+2q) \end{bmatrix} \quad (5.18)$$

Defining a new noise, I rewrite (5.14) as

$$\mathcal{Y}_k = \mathcal{G}_k \mathcal{X}_k + \tilde{\mathcal{Z}}_k \quad (5.19)$$

where

$$\tilde{\mathcal{Z}}_k \triangleq \mathcal{G}_k^{upper} \mathcal{X}_{k-q}^{upper} + \mathcal{G}_k^{lower} \mathcal{X}_{k+q}^{lower} + \mathcal{Z}_k. \quad (5.20)$$

If I design a block linear filter of dimension $(4q+2) \times (4q+2)$ and apply to (5.19), I obtain

$$\mathbf{V}_k \mathcal{Y}_k = \underbrace{\mathbf{V}_k \mathcal{G}_k}_{\triangleq \tilde{\mathcal{G}}_k} \mathcal{X}_k + \mathbf{V}_k \tilde{\mathcal{Z}}_k. \quad (5.21)$$

Similar to the TDBLF case, I desire that $\bar{\mathcal{G}}_k$ becomes a diagonal matrix.

To derive an SINR expression, I consider the noise power first.

$$\mathbf{E} \left\{ \left| \tilde{z}_k(p) \right|^2 \right\} \triangleq \mathbf{E} \left| \mathbf{e}_p^H \mathbf{V}_k \tilde{\mathcal{Z}}_k \right|^2 \quad (5.22)$$

$$= \mathbf{v}_{k,p}^H \mathbf{E} \left\{ \tilde{\mathcal{Z}}_k \tilde{\mathcal{Z}}_k^H \right\} \mathbf{v}_{k,p} \quad (5.23)$$

The above covariance matrix becomes

$$\begin{aligned} \mathbf{E} \left\{ \tilde{\mathcal{Z}}_k \tilde{\mathcal{Z}}_k^H \right\} &= \mathbf{E} \left\{ (\mathcal{G}_k^{upper} \mathcal{X}_{k-q} + \mathcal{G}_k^{lower} \mathcal{X}_{k+q} + \mathcal{Z}_k) \right. \\ &\quad \cdot (\mathcal{G}_k^{upper} \mathcal{X}_{k-q} + \mathcal{G}_k^{lower} \mathcal{X}_{k+q} + \mathcal{Z}_k)^H \left. \right\} \end{aligned} \quad (5.24)$$

$$\begin{aligned} &= \sigma_z^2 \mathbf{I}_{4q+2} + E_s \cdot \left\{ \mathcal{G}_k^{lower} \mathcal{G}_k^{lower H} \right\} \\ &\quad + E_s \cdot \left\{ \mathcal{G}_k^{upper} \mathcal{G}_k^{upper H} \right\}. \end{aligned} \quad (5.25)$$

Considering the off-diagonal terms of $\bar{\mathcal{G}}_k$ as interference, I desire that the FDBLF maximizes the following $SINR_{f,k}(p)$

$$SINR_{f,k}(p) \triangleq \frac{E_x |\mathbf{e}_p^H \bar{\mathcal{G}}_k \mathbf{e}_p|^2}{\mathbf{v}_{k,p}^H \mathbf{E} \left\{ \tilde{\mathcal{Z}}_k \tilde{\mathcal{Z}}_k^H \right\} \mathbf{v}_{k,p} + E_x \sum_{m \neq k} |\mathbf{e}_p^H \bar{\mathcal{G}}_k \mathbf{e}_m|^2} \quad (5.26)$$

where the vector \mathbf{e}_p is now a unit norm column vector of length $(4q+2)$ with the p -th element of 1.

I can formulate the following optimization problem that is similar to

(2.31)

For each $k = q, q + 1, \dots, 2N - q$

For $p = q, 3q + 1$

$$\begin{aligned} \max_{\mathbf{v}_{k,p}} \mathbf{v}_{k,p}^H \mathbf{g}_p \mathbf{g}_p^H \mathbf{v}_{k,p} &= 1 \\ \text{subject to } \mathbf{v}_{k,p}^H \left(\frac{\sigma_z^2}{E_x} \mathbf{I}_{4q+2} + \mathcal{R}_{k,p} \right) \mathbf{v}_{k,p} &= 1 \end{aligned} \quad (5.27)$$

where $\mathbf{v}_{k,p} \triangleq \mathbf{V}_k^H \mathbf{e}_p$, $\mathbf{g}_{k,p} \triangleq \mathcal{G}_k \mathbf{e}_p$, and $\mathcal{R}_{k,p} \triangleq \mathcal{G}_k \mathcal{G}_k^H - \mathbf{g}_{k,p} \mathbf{g}_{k,p}^H + \mathcal{G}_k^{lower} \mathcal{G}_k^{lower H} + \mathcal{G}_k^{upper} \mathcal{G}_k^{upper H}$.

The above optimization problem is solved as follows.

For each $k = 0, 1, \dots, N - 1$

For each $p = q, 3q + 1$

$$\mathcal{R}_k = \frac{\sigma_z^2}{E_x} \mathbf{I}_{4q+2} + \mathcal{G}_k \mathcal{G}_k^H + \mathcal{G}_k^{lower} \mathcal{G}_k^{lower H} + \mathcal{G}_k^{upper} \mathcal{G}_k^{upper H} \quad (5.28)$$

$$\mathbf{g}_{k,p} = \mathcal{G}_k \mathbf{e}_p \quad (5.29)$$

$$\tilde{\mathbf{v}}_p = \mathcal{R}_k^{-1} \mathbf{g}_{k,p} \quad (5.30)$$

$$\mathbf{v}_{p,opt} = \tilde{\mathbf{v}}_p / |\tilde{\mathbf{v}}_p| \quad (5.31)$$

$$\mathbf{V}(k; :) = \mathbf{v}_{q,opt}^T \quad (5.32)$$

$$\mathbf{V}(k + N; :) = \mathbf{v}_{3q+1,opt}^T \quad (5.33)$$

The dimension of the matrix to be inverted (5.30) is $(4q + 2) \times (4q + 2)$ that is much smaller than in time domain filter design process. After obtaining

the above frequency domain filter, transmitted signals are estimated as

For each $k = 0, 1, \dots, N - 1$

$$\hat{X}(k) = \frac{\mathbf{V}(k; :)\mathcal{Y}_k}{\overline{\mathcal{G}}_k(q, q)} \quad (5.34)$$

$$\hat{X}(k + N) = \frac{\mathbf{V}(k + N; :)\mathcal{Y}_k}{\overline{\mathcal{G}}_k(3q + 1, 3q + 1)}. \quad (5.35)$$

5.3 Receiver Combining for Multiple Receive Antennas

When more than one receive antennas exist, an appropriate combining of the received signals is necessary. Although any combining method such as selection combining and switched combining could be used, I adopt the maximal ratio receiver combining (MRRC) since it shows the best performance. If I assume two receive antennas, transmitted signals are estimated as

For each $k = 0, 1, \dots, N - 1$

$$\hat{X}(k) = \frac{\sum_{j=1}^2 \overline{\mathcal{G}}_{i,k}^*(q, q) \mathbf{V}_j(k; :)\mathcal{Y}_{j,k}}{\sum_{j=1}^2 |\overline{\mathcal{G}}_{j,k}(q, q)|^2} \quad (5.36)$$

$$\hat{X}(k + N) = \frac{\sum_{j=1}^2 \overline{\mathcal{G}}_{i,k}^*(3q + 1, 3q + 1) \mathbf{V}_j(k + N; :)\mathcal{Y}_{j,k}}{\sum_{j=1}^2 |\overline{\mathcal{G}}_{j,k}(3q + 1, 3q + 1)|^2} \quad (5.37)$$

where $j = 1, 2$ indicates the receive antenna index. Note that the filter design and filtering process for multiple receive antenna system is the same as the single receive antenna system.

5.4 Complexity Comparison

This section compares the previous TDBLF and the proposed FDBLF in terms of computational complexity. I assume one receive antenna because more than one receive antenna does not change the relative complexity of the two schemes. First, I compare the design complexity of the TDBLF (2.32) and FDBLF (5.30). As can be seen in (2.32), TDBLF requires a $2N \times 2N$ matrix inversion ($(2N)^3$ multiplications) and a matrix vector multiplication ($(2N)^2$) for each $k = 0, 1, \dots, 2N - 1$. If I include the cost of \mathbf{R} matrix construction ($(2N)^3$) and the operation (2.34) ($(2N)^3$), the design of a time domain block-linear filter costs $4 \times (2N)^3$ multiplications in total. The frequency domain filter design procedure requires a $(4q + 2) \times (4q + 2)$ matrix inversion ($(4q + 2)^3$) and a matrix vector multiplication ($(4q + 2)^2$) for each $k = 0, 1, \dots, N - 1$. If I include the cost of \mathcal{R}_k matrix construction ($(4q + 2)^3 + 8q^3$), frequency domain block-linear filter design costs $N[3(4q + 2)^3 + 8q^3 + 2(4q + 2)^2]$ multiplications in total.

Now I compare the filtering process (2.35), (5.34), and (5.35). The time domain filtering costs $(2N)^2$ multiplications and the frequency domain filtering costs $2N(4q + 2)$ multiplications. Combining the costs of filter design and filtering procedures, I can express the ratio of the computational complexity of the two schemes as

$$\begin{aligned} R(q, N) &\triangleq \frac{\text{FDBLF Cost}}{\text{TDBLF Cost}} \\ &= \frac{2(4q + 2)^3 + 8q^3 + 2(4q + 2)^2 + 2(4q + 2)}{32N^2 + 4N}. \end{aligned} \quad (5.38)$$

Table 5.1: Complexity comparison of the FDBLF and the TDBLF.

	Time Domain Block Linear Filter	
Filter Design	\mathbf{R} Construction	$(2N)^3$
	\mathbf{R}^{-1}	$(2N)^3$
	$\mathbf{R}^{-1}\mathbf{h}_k, \forall k$	$(2N)^3$
	\mathbf{W}_t Construction	$(2N)^3$
Filtering	Eq.(2.35)	$(2N)^2$
Total	$4 \times (2N)^3 + (2N)^2$	
	Frequency Domain Block Linear Filter	
Filter Design	$\mathcal{R}_k, \forall k$ Construction	$[(4q+2)^3 + 8q^3]N$
	$\mathcal{R}_k^{-1}, \forall k$	$(4q+2)^3 N$
	$\mathcal{R}_k^{-1}\mathbf{g}_{k,p}, \forall k$	$2(4q+2)^2 N$
	\mathbf{V} Construction	0
Filtering	Eq.(5.34) and (5.35)	$2(4q+2)N$
Total	$[2(4q+2)^3 + 8q^3 + 2(4q+2)^2 + 2(4q+2)]N$	

The computational complexity is summarized in Table 5.1. I note that when a Doppler frequency is fixed, the normalized Doppler frequency decreases as the FFT size decreases and that when the normalized Doppler frequency is small, a smaller q can be used because $2q$ is the number of nearest subchannels causing interchannel interference. Therefore, a smaller N indicates a smaller required q .

5.5 Simulation Results

In this section, I provide simulation results to compare the error performance of the time domain and the frequency domain block-linear filters.

The FFT size N is 128 and CP length ν is 32. The spectral bandwidth

$(1/T_s)$ is $400kHz$. I consider a very high Doppler frequency of $297Hz$ which leads to $f_D(N + \nu)T_s = 0.1188$. Since different signal detection algorithm may react differently to CSI estimation error, I consider both cases when exact CSI is assumed to be known and when CSI is estimated. For the CSI estimation, the pilot tone placement and interpolation method in [38] is adopted.

Fig. 5.3 shows the bit error rate (BER) vs. signal-to-noise ratio (SNR) performance of the simple Alamouti decoding, the previous time domain block-linear filter, and the proposed frequency domain block-linear filter when ideal CSI is assumed to be known. Two transmit antennas and one receive antenna system is considered. As can be observed in Fig. 5.3, the Alamouti decoding shows the worst performance and the time domain block-linear filter achieves the best performance. The proposed frequency domain block-linear filter with different $q(q = 1, 3, 4)$ falls between the two schemes. As the parameter q increases from 1 to 4, the performance of the frequency domain filter gets closer to that of the time domain block-linear filter. The performance gap between the time domain and the frequency domain filter approaches seems to be due in part to the block diagonal approximation.

Fig. 5.4 shows the performance of the three schemes when CSI is estimated. Again, the Alamouti decoding shows the worst performance and the time domain filtering shows the best performance. Unlike in the ideal CSI case, however, the proposed frequency domain filter with $q = 4$ shows almost identical performance with the time domain filter for SNR range from 5 up to $25dB$. This is because the time domain filter approach is more sensitive to

CSI estimation error than the proposed frequency domain filter approach is. There still exist performance gap between the two schemes when SNR is as high as $30dB$.

Fig. 5.5 shows a coded BER performance (CSI is estimated) of the Alamouti decoding, proposed FDBLF ($q=1,3,4$), and the previous TDBLF. The $1/2$ rate convolutional coding and corresponding Viterbi decoding (constraint length of 3, storage depth of 64) is used in conjunction with bit level interleaving. Comparing Fig. 5.4 and 5.5, significant coding gain of all the decoding methods can be observed. At the target BER of 10^{-3} , the coding gain of the proposed FDBLF ($q = 4$) is as big as $15dB$. The relative performance of the various decoding schemes stays almost the same as in Fig. 5.4.

Fig. 5.6 is the BER performance of the three schemes when CSI is estimated. Two transmit antenna and two receive antenna OFDM system with maximal ratio receive combining (MRRC) is considered. Again, the performance of the proposed frequency domain filter falls between the previous TDBLF and the Alamouti decoding. The proposed scheme with $q = 4$ shows almost identical performance as the previous time domain filter over entire considered SNR range. However, the performance gap of the proposed schemes with different q 's is quite different from the one receive antenna case. The proposed scheme with $q = 1$ shows a very small performance degradation relative to $q = 4$ case. It seems that the increased diversity gain employing two receive antennas is a dominant factor in the performance improvement over one receive antenna system. Therefore, a smaller q for the proposed frequency

domain filter is desirable when two receive antennas are used than when one receive antenna is used.

Comparing fig.5.4 and 5.6, it can be observed that the simple Alamouti decoding improves the error performance significantly by employing one more receive antenna at the receiver. The time domain filtering approach requires the SNR of $26.5dB$ to achieve BER of 10^{-3} when one receive antenna is used, while the Alamouti decoding requires SNR of only $21dB$ to achieve BER of 10^{-3} when two receive antennas are used. Therefore, depending on the target BER, the cost of one more receive antenna, and computational complexity, the simple Alamouti decoding may be a preferred choice even in quite fast fading channels.

Finally, I evaluate the complexity cost ratio using parameters adopted in the simulations. Table 5.2 shows the complexity ratio of the two schemes for various q and a fixed N . As the parameter q increases, the ratio decreases. Even when the parameter $q = 4$ that is the maximum value adopted in the simulations, the proposed FDBLF complexity is approximately $1/41$ of TDBLF. Therefore, I can conclude that the proposed frequency domain block-linear filter is computationally much more efficient at the cost of a small performance degradation, compared with the previous time domain filter.

5.6 Conclusions

This chapter proposes a frequency domain block-linear filter to mitigate the time-varying channel effects in MIMO OFDM systems in a computationally

Table 5.2: Complexity ratio of the FDBLF to the TDBLF for various q .

$N = 128$	$q = 1$	$q = 2$	$q = 3$	$q = 4$
$R(q, N)$	$\frac{1}{1000}$	$\frac{1}{230}$	$\frac{1}{86}$	$\frac{1}{41}$

efficient manner. The frequency domain block-linear filter is based on the sparse structure of the system matrix in the frequency domain. I showed that the proposed frequency domain filtering is computationally much more efficient than the previous time domain filtering. Simulation results showed that although performance gap between the two schemes exist when ideal CSI is assumed to be known, the performance gap becomes almost negligible when the CSI is estimated, which implies the robustness of the proposed scheme to CSI estimation error. I also showed that the simple Alamouti decoding might be a preferred choice even in fast fading channels, depending on various system design factors.

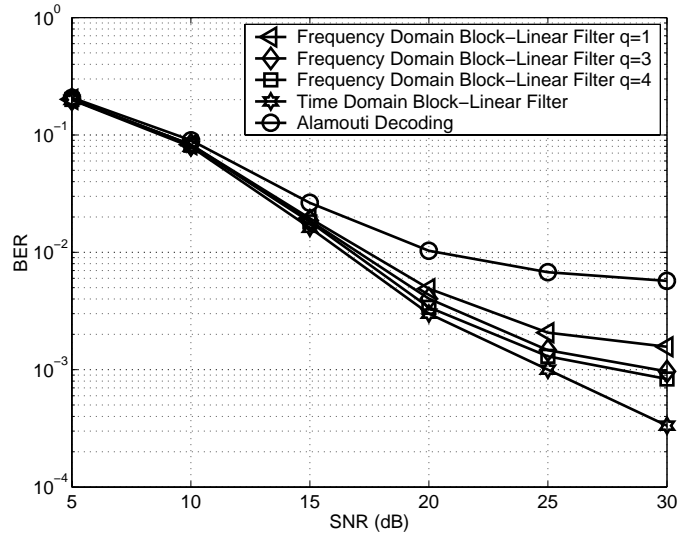


Figure 5.3: BER performance of the Alamouti decoding, the previous time domain block-linear filter, and the proposed frequency domain block-linear filter when ideal CSI is assumed to be known. Two transmit antennas and one receive antenna OFDM system.

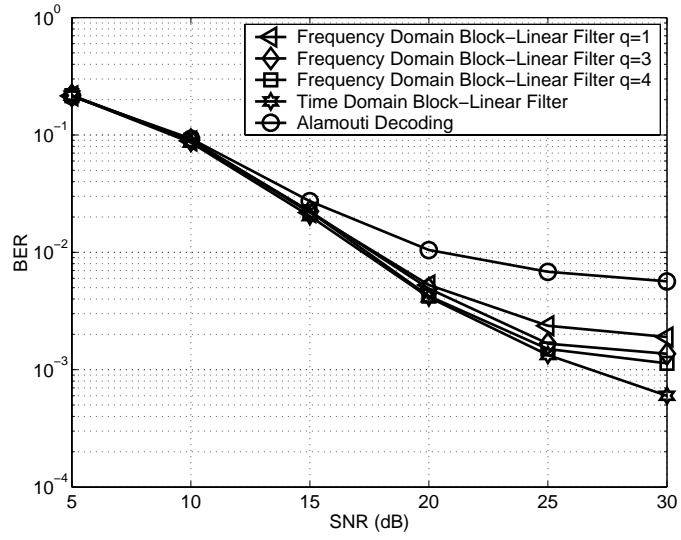


Figure 5.4: BER performance of the Alamouti decoding, the previous time domain block-linear filter, and the proposed frequency domain block-linear filter when CSI is estimated. Two transmit antennas and one receive antenna OFDM system.

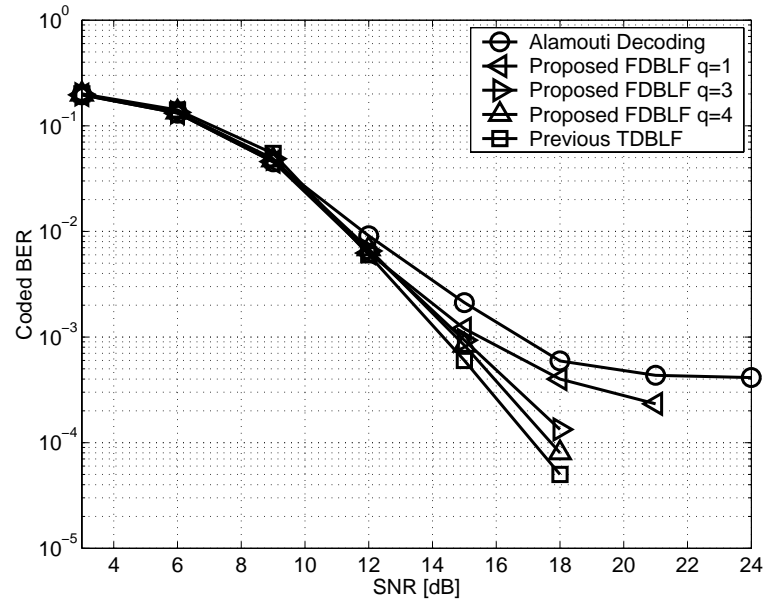


Figure 5.5: Coded BER performance (estimated CSI) of the Alamouti Decoding, proposed FDBLF($q = 1, 3, 4$), and the Time Domain MMSE. Convolutional coding of rate $1/2$ is used in conjunction with a bit level interleaving.

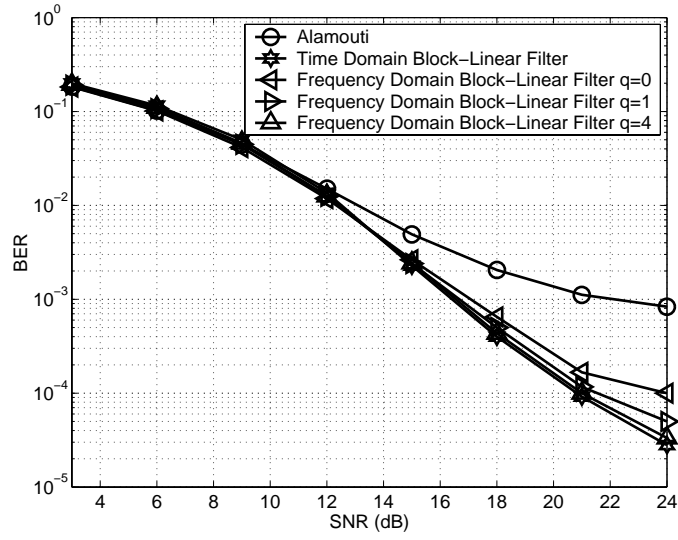


Figure 5.6: BER performance of the Alamouti decoding, the previous time domain block-linear filter, and the proposed frequency domain block-linear filter when CSI is estimated. Two transmit antennas and two receive antennas OFDM system with maximal ratio receive combining (MRRC).

Chapter 6

Bandwidth Efficient OFDM Transmission

In this chapter, OFDM systems without cyclic prefix in indoor wireless channels are addressed. Two compensation techniques are described, a previous technique in Sec.6.2 and a proposed technique in Sec.6.3 [63]. Sec.6.4 provides simulation results to show the improved performance of the proposed technique.

6.1 OFDM without Cyclic Prefix

In this chapter, only static multipath channels are considered. This is usual for indoor channels because only negligible Doppler shift exists in the indoor environment. Correct channel estimation and correct synchronization are assumed. The same system is considered that is described in chapter 1. However, I consider only the case when $\nu = 0$, i.e., spectral efficiency is 1. Then (1.5) changes to

$$r_i[n] = \sum_{m=0}^{M-1} h[m]x_i[n-m]u[n-m] + \sum_{m=0}^{M-1} h[m]x_{i-1}[n+N-m](1-u[n-m]) \quad (6.1)$$

where $u[\cdot]$ represents the unit step function. The second term of (6.1) represents the ISI terms due to the absence of CP. When $\nu = 0$, ISI and ICI occurs,

degrading OFDM system performance. Two approaches to resolve this problem are described in the next sections, a previous approach and a new proposed approach in this chapter.

6.2 Previous Iterative Signal Detection Method

An iterative technique, called residual ISI cancellation (RISIC) [64], uses a combination of tail cancellation and cyclic restoration. The RISIC algorithm proceeds as follows.

Step 1) Decision on the transmitted symbols $X_{i-1}[k], 0 \leq k \leq N-1$, is made. These symbols are converted back to the time domain using IFFT giving

$$x_{i-1}[n] = \frac{1}{\sqrt{N}} \sum_{k=0}^{N-1} X_{i-1}[k] e^{j2\pi kn/N}. \quad (6.2)$$

Step 2) Tail cancellation is performed as follows.

$$\begin{aligned} \tilde{r}_i[n]^{(0)} = r_i[n] & - \sum_{m=\nu+1}^M h[m] x_{i-1}[(n-m)_N] \\ & \cdot (1 - u[n-m]), 0 \leq n \leq N-1. \end{aligned} \quad (6.3)$$

Step 3) The $\tilde{r}_i[n]^{(0)}, 0 \leq n \leq N-1$, obtained in Step 2 are converted to the frequency domain. Frequency domain 1-tap equalization is done as

$$\hat{X}_i[k]^{(0)} = FFT_N\{\tilde{r}_i[n]^{(0)}\}/H[k] \quad (6.4)$$

where $H[k] = FFT_N\{h_n\}$. After decision is made, IFFT is again applied to the decisions to give $\hat{x}_i[n], 0 \leq n \leq N-1$.

Step 4) Cyclic reconstruction is performed

$$\begin{aligned} \tilde{r}_i[n]^I = \tilde{r}_i[k]^{(0)} &+ \sum_{\nu+1}^M h[m] \hat{x}_i[(n-m)_N]^{I-1} \\ &\cdot (1 - u[n-m]), 0 \leq n \leq N-1. \end{aligned} \quad (6.5)$$

Step 5) The $\tilde{r}_i[n]^{(I)}, 0 \leq n \leq N-1$ are converted to the frequency domain, frequency domain equalization is done, and decisions are made yielding $\hat{X}_i[k]^{(I)}, 0 \leq k \leq N-1$. This is the end of I -th iteration in the RISIC algorithm.

Step 6) To continue iterations, the $\hat{X}_i[k]^{(I)}, 0 \leq k \leq N-1$, is converted to $\hat{x}_i[n]^{(I)}, 0 \leq n \leq N-1$, and repeat Steps 4-6 with $I \leftarrow I+1$.

In step 3 and step 5, intermediate decisions are made to be used in the following steps. Spectral nulls lead to degradation of these intermediate decisions, resulting in more required iterations.

6.3 Proposed Signal Detection Method

In this section, a new proposed approach is described. Fig.6.1 shows the block diagram of the proposed approach which proceeds as follows:

Step 1) Optimal delay is estimated.

$$D = \arg \max_{d \in \{0,1,\dots,N-2\nu\}} \left\{ \sum_{n=0}^{N-2\nu} |z[(N-d+n)_N]| \right\} \quad (6.6)$$

where $z[n] = IFFT_N\{1/H[k]\}, 0 \leq n \leq N-1$.

Step 2) Tail portion (ν samples) of the current block is recovered.

$$\hat{X}_i[k]' = FFT_N\{\mathbf{r}\}/H[k] \quad (6.7)$$

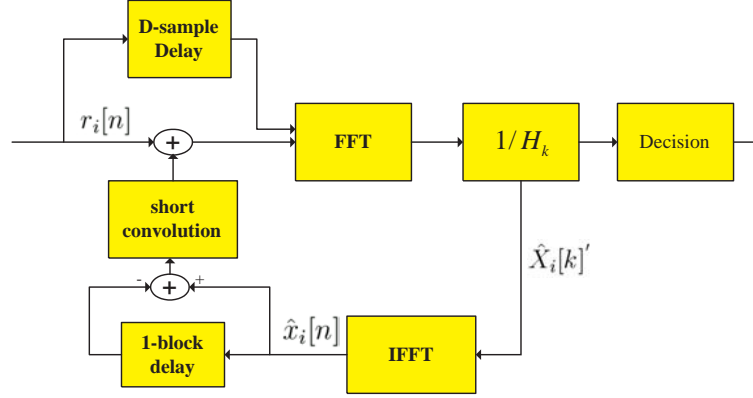


Figure 6.1: Block diagram of the proposed method for OFDM transmission without cyclic prefix.

where $\mathbf{r} = [r_i[D], r_i[D + 1], \dots, r_i[N - 1], r_{i+1}[0], \dots, r_{i+1}[D - 1]]$.

$\hat{X}'_{i,k}$ is converted back to time domain giving $\hat{x}_i[n]', 0 \leq n \leq N - 1$.

Step 3) Tail cancellation and cyclic reconstruction are performed simultaneously.

$$\tilde{r}_i[n] = r_i[n] + h[n] * (\hat{x}_i[N - M + n]' - \hat{x}_{i-1}[N - M + n]') \quad (6.8)$$

where $*$ stands for linear convolution.

Step 4) $\tilde{r}_i[n], 0 \leq n \leq N - 1$, are converted to the frequency domain. Frequency domain equalization is done and decisions are made yielding $\hat{X}_i[k], 0 \leq k \leq N - 1$.

Although one block delay is introduced in Step 2, no intermediate decisions are used in the proposed scheme. Therefore, the proposed scheme is robust to the occurrence of spectral nulls. Furthermore, the proposed approach is computationally efficient in that no more than 1 iteration is required regardless of the existence of spectral null.

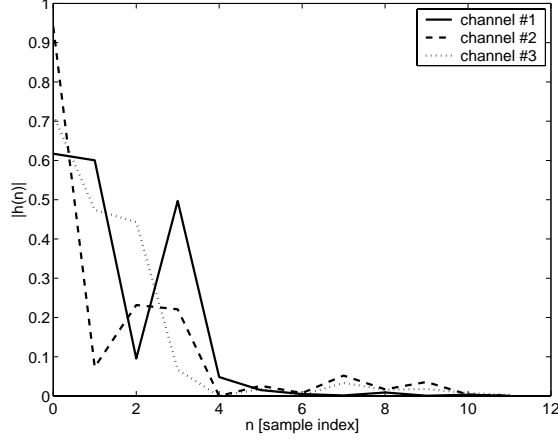


Figure 6.2: Indoor channels used in Chapter 6 simulations.

6.4 Simulation Results

In this section, a simulation experiment is conducted to validate the proposed approach. The constellation used in the simulation is 16-QAM. The number of subcarriers is 128. Typical multipath indoor channels used in the simulation are shown in Fig.6.2 [65]. The delay spread of the channels is 11 samples. The frequency selectivity of those channels is shown in Fig.6.3. As can be observed in Fig.6.3, channel #2 has the most moderate spectral null, channel #3 has the deepest spectral null, and the channel #1 is between them. The previous approach and the proposed one are compared in terms of Symbol Error Rate (SER) vs. Signal-to-Noise Ratio (SNR).

Fig.6.4 compares the RISIC algorithm and the proposed approach when the channel #1 is used. Channel #1 has a moderate spectral null and the frequency domain null requires at least 3 iterations for the RISIC algorithm.

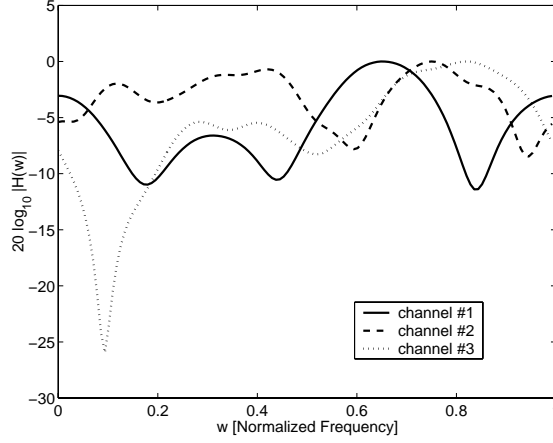


Figure 6.3: Frequency selectivity of the indoor channels

The proposed approach works well, showing a little bit better performance than RISIC with $I = 3$

Fig.6.5 compares the RISIC algorithm and the proposed approach when the channel #2 is used. Channel #2 has the most moderate spectral null among the three in Fig.6.3. As can be observed, RISIC works well even with just 1 iteration. The proposed approach shows almost the same performance as the RISIC algorithm.

Fig.6.6 compares the RISIC algorithm and the proposed approach when the channel #3 is used. Channel #3 has the deepest spectral null among the three in Fig.6.3. As can be observed in Fig.6.6, when there exists a deep spectral null, the RISIC approach does not work well even after considerable computation with iteration number 3. But the proposed approach works well regardless of the existence of the spectral null. Therefore, I can say that the

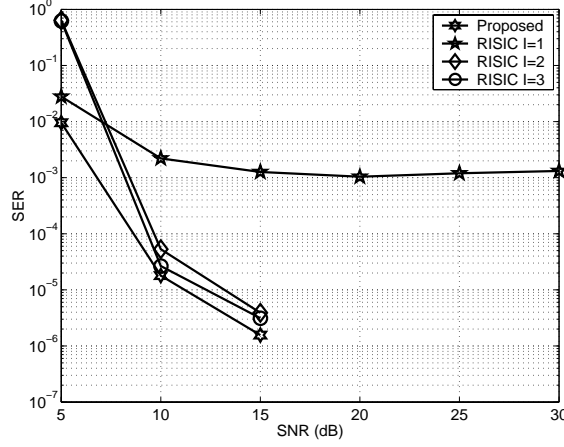


Figure 6.4: SER performance of the previous RISIC and the proposed signal detection algorithm for OFDM systems without cyclic prefix when channel #1 is used.

proposed approach is robust to the presence of spectral nulls. Furthermore, the proposed approach is computationally efficient because no more than one iteration is required.

6.5 Conclusions

In this chapter, a new bandwidth efficient OFDM transmission scheme is proposed. Although the proposed approach introduces a block delay, it is robust to spectral nulls because no intermediate decision is used. Furthermore, the proposed approach is computationally efficient in that no more than one iteration is required regardless of the existence of the spectral null of the channel. Simulation experiment results show that the proposed approach outperforms the RISIC approach in the presence of spectral nulls.

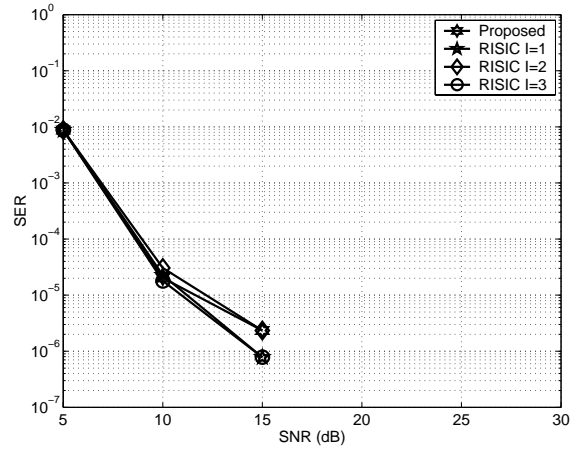


Figure 6.5: SER performance of the previous RISIC and the proposed signal detection algorithm for OFDM systems without cyclic prefix when channel #2 is used.

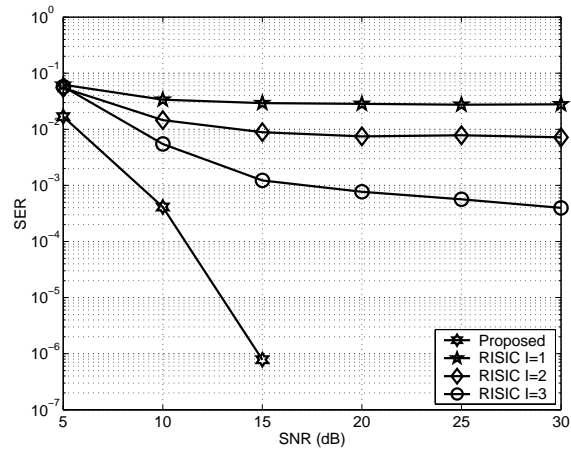


Figure 6.6: SER performance of the previous RISIC and the proposed signal detection algorithm for OFDM systems without cyclic prefix when channel #3 is used.

Chapter 7

Non-Synchronized Sampling System

In this chapter, it is shown that the idea of subsymbol equalization, the technique used for OFDM transmission without cyclic prefix in chapter 6, can also be successfully applied for timing error correction in non-synchronized sampling systems [66]. In Sec.7.1, non-synchronized sampling DMT system is introduced. Sec.7.2 analyzes the timing error effect in non-synchronized sampling DMT systems. Sec.7.3 proposes a timing error correction scheme. Simulation results are provided in Sec.7.4.

7.1 DMT with Non-Synchronized Sampling

In synchronized sampling systems, a voltage controlled oscillator (VCO) is used for sampling time generation at the receiver. A block diagram of a synchronized sampling system is given in Fig.7.1. As can be seen in Fig.7.1, estimated timing error is fed back to the VCO to adjust the sampling time accordingly.

However, in non-synchronized sampling systems using a fixed free-running crystal, the timing error correction is done in the digital domain without feedback to the analog domain. The corresponding block diagram is given

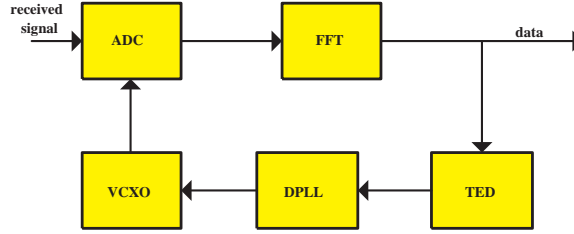


Figure 7.1: Block diagram of synchronized sampling DMT systems.

in Fig.7.2. The effect of sampling time error is serious for non-synchronized sampling OFDM/DMT systems especially when a long OFDM/DMT symbol is used [67]. A digital timing error correction scheme combining temporal and spectral signal properties was proposed [68][69]. In this approach, time domain interpolation is used in conjunction with the frequency domain rotor to correct the timing error. But the time domain interpolation requires over-sampling at the analog front end, which is not suitable for high-speed systems. Furthermore, the time domain/ frequency domain hybrid approach [68][69] assumes moderate OFDM/DMT symbol length. Therefore, a computationally efficient scheme that works regardless of symbol length is necessary.

In this chapter, a new computationally efficient frequency domain timing error correction scheme without time domain interpolation is proposed. Furthermore, the proposed approach works well regardless of the length of the OFDM/DMT symbol. A DMT system is used as an example platform for the simulation.

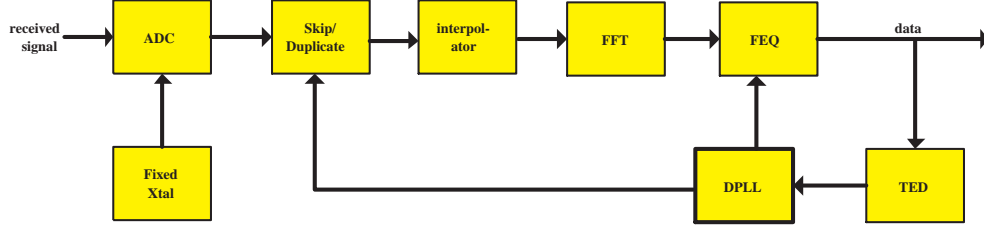


Figure 7.2: Block diagram of non-synchronized sampling DMT systems.

7.2 Timing Error in Non-synchronized Sampling Systems

In this section, I discuss the impact of sampling frequency offset (SFO) at the receiver sampling device. The DMT time domain signal at the receiver, can be expressed as

$$r(t) = \frac{1}{2N} \sum_{m=-\infty}^{\infty} \sum_{k=0}^{2N-1} X_m[k] g_m^k(t) + n(t) \quad (7.1)$$

with

$$g_m^k(t) = \sum_{n=-\nu}^{2N-1} g(t - (m(2N + \nu) + n)T) e^{j \frac{2\pi}{2N} kn} \quad (7.2)$$

where $g(t)$ stands for the composite channel impulse response including the transceiver filters and the channel; $X_m[k] = X_m^*[2N - k]$, $1 \leq k \leq N - 1$, is the QAM symbol modulating the k -th carrier in the m -th symbol where $*$ means complex conjugate; N is the number of carriers in the DMT system; T is the sample period at the transmitter; and $n(t)$ the additive noise [69]. I assume an ideal channel impulse response and ideally band-limiting transceiver filters. This continuous time signal is inputted to the receiver sampling device. If the received symbol is aligned by the frequency domain rotor whose angle

is $-2\pi\frac{k}{2N}\{\delta(1 - \frac{\Delta f}{f_s}) - [m(2N + \nu) + N + 0.5]\frac{\Delta f}{f_s}\}$, then the estimated time domain symbol is given as the sum of useful data rotated and attenuated and interference from other samples. The variance of interference from other samples (IsI) can be derived in a way similar to the variance of ICI in [1], which yields

$$Var[IsI] \approx E [|s_m[l]|^2] \frac{1}{4N^2} \sum_{l=0, l \neq n}^{2N-1} \frac{[\pi(N + 0.5 - n)]^2}{\sin^2 [\frac{\pi}{2N}(n - l)]} \left(\frac{\Delta f}{f_s}\right)^2 \quad (7.3)$$

where, Δf is the SFO and δ is an integer such that $|\epsilon_m^0| \leq 0.5$ where ϵ_m^0 is given as $\delta - [m(2N + \nu) + \delta]\frac{\Delta f}{f_s}$, and $X_m[k] = \sum_{l=0}^{2N-1} s_m[l]e^{-j2\pi kl/2N}$.

The variance of the IsI is approximately proportional to the square of $|N + 0.5 - n|$, the distance from the center point with frequency offset fixed.

7.3 Proposed Timing Error Correction Scheme

In this section, a proposed timing error correction scheme is described. Let $\tilde{S}_m = [\tilde{s}_m[0], \tilde{s}_m[1], \dots, \tilde{s}_m[2N-1]]$ be the current block after the sampling with timing error. This block is partitioned into P short sub-symbols. $N - \frac{N}{P}$ samples in the previous sub-symbol and $N - \frac{N}{P}$ samples in the next sub-symbol are used, making the p -th sub-symbol (\tilde{S}_{mp}) of length $2N$. This is where a one block delay is introduced. Frequency domain timing error correction is done

for each sub-symbol. This procedure can be described as follows.

For each $p \in \{0, 1, \dots, P-1\}$

$$Z_{mp}[k] = DFT_{2N}\{\tilde{S}_{mp}\}$$

Rotation of $Z_{mp}[k]$ by $\tilde{\epsilon}_{mp}$

$$z_{mp}[n] = IDFT_{2N}\{Z_{mp}[k]\}$$

where $\tilde{\epsilon}_{mp}$ is the average timing error for the p -th partition of the m -th symbol.

The average timing error, $\tilde{\epsilon}_{mp}$, is expressed as

$$\tilde{\epsilon}_{mp} = \frac{2N}{P} \sum_{n=0}^{\frac{2N}{P}-1} \epsilon_m^{n + \frac{2N}{P}p}. \quad (7.4)$$

And the estimated time domain symbol, $\hat{S}_m = [\hat{s}_m[0], \hat{s}_m[1], \dots, \hat{s}_m[2N-1]]$,

is given as

$$\begin{aligned} \hat{S}_m = & \left[z_{m1} \left[\frac{2N}{P} \frac{P-1}{2} - 1 \right], \dots, z_{m1} \left[\frac{2N}{P} \frac{P+1}{2} - 1 \right], \right. \\ & z_{m2} \left[\frac{2N}{P} \frac{P-1}{2} - 1 \right], \dots, z_{m2} \left[\frac{2N}{P} \frac{P+1}{2} - 1 \right], \\ & \left. \dots, z_{mP} \left[\frac{2N}{P} \frac{P-1}{2} - 1 \right], \dots, z_{mP} \left[\frac{2N}{P} \frac{P+1}{2} - 1 \right] \right]. \quad (7.5) \end{aligned}$$

The estimated symbol \hat{S}_m is fed to the demodulating FFT, producing estimated QAM symbols.

7.4 Simulation Results

In this section, the proposed scheme is verified through simulation. The FFT size is 1024. A cyclic prefix of 32 samples is used. The values, $P = 8$

and $N = 512$, are used for the proposed approach. A 16-QAM constellation is used for each sub-channel. An SNR of $30dB$ in the time domain and correct timing error detection are assumed. A raised cosine filter with roll off factor of 0.03 is used as the transmit and receive filter. The criterion used to verify the proposed scheme is the normalized mean square error (NMSE) defined as

$$NMSE = \frac{E [|s_m[n] - \hat{s}_m[n]|^2]}{E [|s_m[n]|^2]}. \quad (7.6)$$

where $s_m[n]$ denotes the true value and $\hat{s}_m[n]$ denotes the estimated value.

Fig. 7.3 shows NMSE's when $N = 512$ and $SFO = 100ppm$. The solid line is the NMSE when the frequency domain rotor is used. The dashed line shows the NMSE when the proposed approach is applied. The proposed scheme with $P = 8$ reduces the ISI in terms of NMSE to the level of less than $-30dB$ for the entire time domain symbol again.

Fig. 7.4 shows the recovered constellations corresponding to Fig.7.3. Fig. 7.4(a) corresponds to the case when the frequency domain rotor is used and Fig. 7.4(b) when the proposed approach with $P = 8$ is applied to the samples with timing error. The proposed approach with $P = 8$ recovers the constellation almost perfectly.

7.5 Conclusions

In this chapter, a new computationally efficient timing error correction scheme is proposed for non-synchronized sampling OFDM/DMT systems. Each OFDM/DMT symbol is partitioned into several short sub-symbols in the

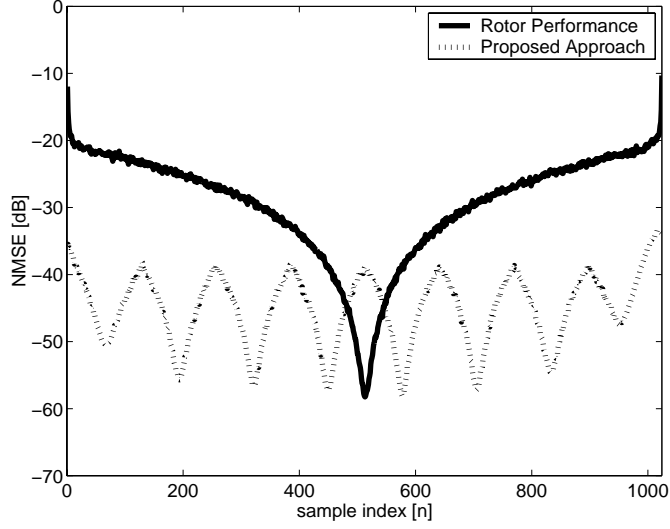
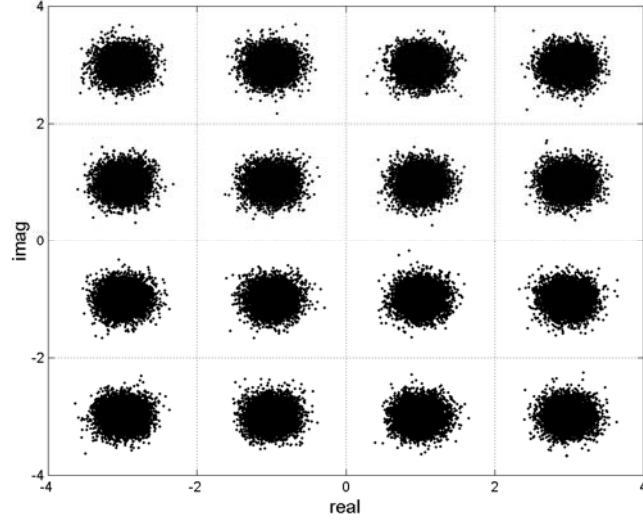
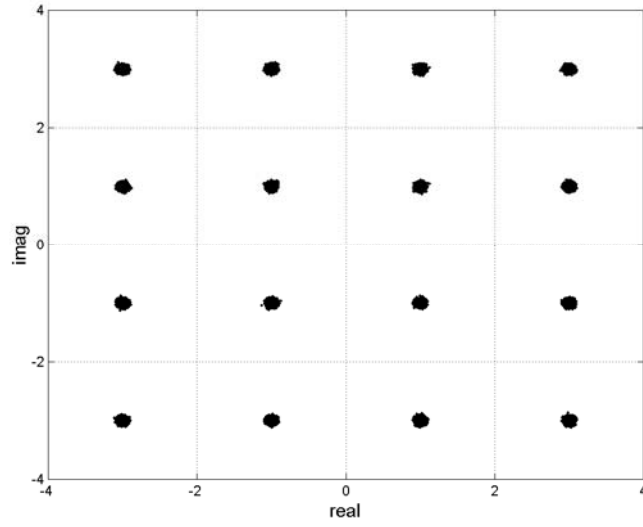


Figure 7.3: NMSE comparison when $N = 512$, $SFO = 100ppm$

time-domain and timing error correction is done for each sub-symbol in the frequency domain using the delay-rotor property. Although the new approach introduces a one block delay it is computationally efficient in that neither over-sampling at the analog front end nor time domain interpolation is involved. Furthermore, the proposed approach works well regardless of the OFDM/DMT symbol length.



(a)



(b)

Figure 7.4: Recovered constellation when $N = 512$, SFO=100ppm (a) frequency domain rotor, (b) proposed approach with $P = 8$

Chapter 8

Conclusions and Future Work

8.1 Conclusions

In this dissertation, I addressed signal detection methods for various OFDM systems.

Chapter 3, 4, and 5 proposed a decision directed receiver, sequence estimation receivers, and frequency domain block linear filtering receiver, respectively, for OFDM systems with transmit diversity in fast fading channels. It was shown in Chapter 3 that decision directed receiver improves the error performance although the improvement is limited to moderate normalized Doppler frequency.

Chapter 4 showed that the sequence estimation receivers offer good trade-off between the complexity and the error performance, compared with the previous time domain block linear filter. The drawbacks of the sequence estimation receivers, however, are that the complexity is time-variant, which is not amenable to hardware implementation, and that the complexity is dependent on the signal constellation size. As a larger constellation is involved, the complexity increases.

In chapter 5, a frequency domain block linear filtering receiver was pro-

posed, whose computational complexity is neither dependent on the constellation size nor time-variant. The proposed frequency domain filter significantly reduces the computational complexity of the previous time domain filter, exploiting the sparse structure of the system matrix in the frequency domain.

Chapter 6 dealt with the OFDM transmission without cyclic prefix for higher bandwidth efficiency. Unlike the previous iterative signal detection method, the error performance of the proposed signal detection method was shown to be robust to spectral nulls. However, the applicability of the proposed approach is limited to the channels without zeros exactly on the unit circle and moderate Doppler frequency.

Chapter 7 dealt with OFDM systems with non-synchronized sampling at the receiver. In non-synchronized sampling systems, sampling time error is compensated in the digital domain without feedback to the analog domain. It was shown that the idea of subsymbol equalization, the technique used for OFDM without cyclic prefix in Chapter 6, can also be successfully used for the timing error correction for the non-synchronized sampling systems.

8.2 Future Work

8.2.1 Equalization for Multi-User OFDM Systems

In the future, I will try to extend the equalization technique for OFDM without cyclic prefix (CP) or with insufficient CP to multi-user OFDM systems that is illustrated in Fig.8.1. Unlike in single user OFDM systems, only a subset of subchannels are allocated to a user in multi-user OFDM systems.

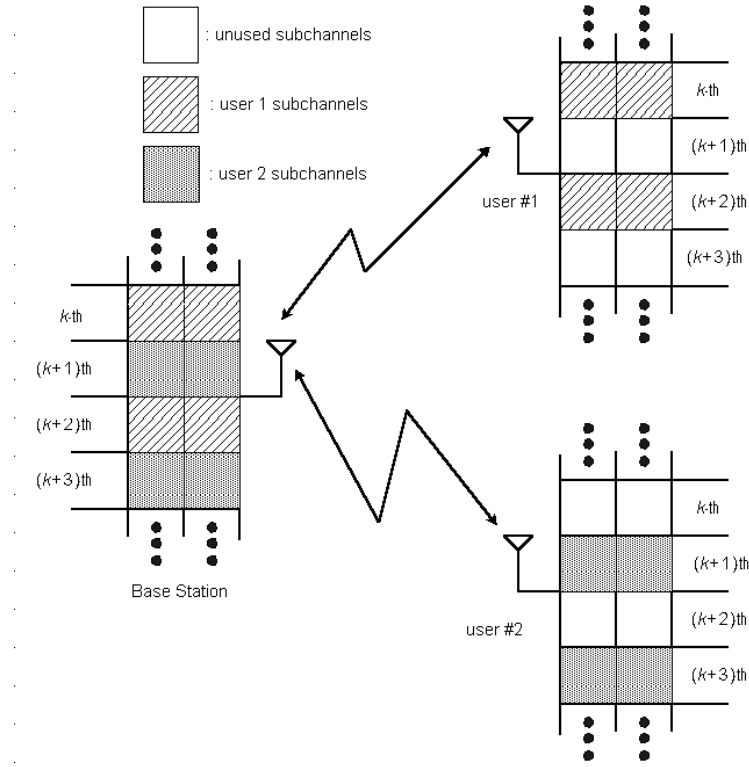


Figure 8.1: Illustration of multi-user OFDM when there exists 2 users.

We can observe in Fig.8.1 that the k -th and the $(k + 2)$ -th subchannels are allocated to the first user. Similarly, the $(k + 1)$ -th and $(k + 3)$ -th subchannels are utilized by the second user.

There exist various methods of subchannel allocation for the multi-user OFDM systems [70][71][72]. A simple subchannel allocation method is that subchannels with high gains are allocated to users [73][74], an approach that may be used in my extension. If the two channels are assumed to be independent of each other, the probability that a subchannel is bad for both users at the same time becomes low. Fig.8.2 provides an example of the

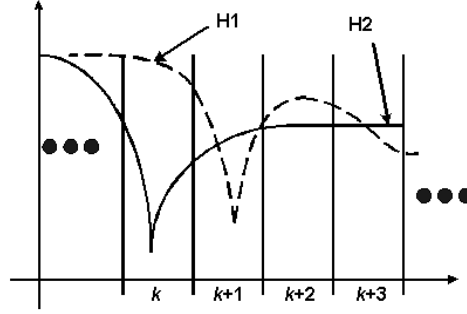


Figure 8.2: Example of subchannel gains in multi-user OFDM systems. Subchannels are assumed to be allocated in the same manner as in Fig.8.1.

simple subchannel allocation. The gain of the channel between the base station and the first (second) user is denoted as $H1$ ($H2$). It was assumed that the subchannels are allocated in the same manner as in Fig.8.1. As can be seen in Fig.8.2, the $(k + 1)$ -th subchannel is bad from the first user's perspective, however, it is good for the second user.

As mentioned in Chapter 6, the proposed OFDM transmission does not work well when there exist spectral nulls or zeros that are close to the unit circle in the wireless channels. However, if only a subset of subchannels are to be equalized and the subchannels do not have deep spectral nulls, as in the multi-user OFDM systems, an optimization technique or interpolation techniques might be successfully adopted to set the unused subchannel gains such that the one tap frequency domain equalizer has a short impulse response in the time domain.

Recently, IEEE 802.16a has been approved as standard of air interface (frequency band of 2-11 GHz) for fixed wireless access [75][76][77], where the

multiuser OFDM is used as multiple access method. Considered ratios of guard time (cyclic prefix length) to the useful time (FFT size) in [75] are 1/32, 1/16, 1/8, 1/4, which are significant overhead. Therefore, the equalization technique in Chapter 6 might be successfully applied to the 802.16 systems.

8.2.2 Extension of SDFSE with an AT

In derivation of $B[k]$ in (4.14), QPSK constellation was assumed. If I remove the assumption, a more general bound is derived as

$$\left\| \sum_{m=k+1}^{\min(k+q, (N+N_c)/2-1)} \mathbf{A}[k, m] \hat{\mathbf{X}}[m] \right\| \leq \|\mathbf{X}\|_{max} \sum_{m=k+1}^{\min(k+q, (N+N_c)/2-1)} \|\mathbf{A}[k, m]\| \triangleq B[k]$$

where $\|\mathbf{X}\|_{max}$ denotes the maximum norm corresponding to a signal constellation. If QPSK is assumed, all constellation points have the same norm. However, if a large constellation in QAM family is used, the maximum norm becomes bigger. Consequently, for a fixed degree of time variation of the channels (fixed $\|\mathbf{A}[k, m]\|$), the bound increases as larger non-constant modulus constellation is involved. As the bound increases, the candidate set \mathcal{S}_k is expected to grow, thereby decreasing the efficiency of the idea of adaptive threshold (AT). Furthermore, I note that if different power is transmitted to subchannels due to either power control or power mask at the transmitter, the bound needs to be changed accordingly.

Therefore, I will search for a more efficient method to set the $B[k]$ without degrading the error performance significantly.

Bibliography

- [1] R. W. Chang, “Synthesis of band-limited orthogonal signals for multi-channel data transmission,” *Bell System Technology Journal*, vol. 46, pp. 1775–1796, Dec. 1966.
- [2] B. R. Saltzberg, “Performance of an efficient parallel data transmission system,” *IEEE Trans. on Commun.*, vol. 15, pp. 805–811, Dec. 1967.
- [3] G. C. Porter, “Error distribution and diversity performance of a frequency differential PSK HF modem,” *IEEE Trans. on Commun.*, vol. 16, pp. 567–575, Aug. 1968.
- [4] M. S. Zimmerman and A. T. Kirsch, “The an/gsc-10 (kathryn) variable rate data modem for HF radio,” *IEEE Trans. on Commun.*, vol. 15, pp. 197–205, Apr. 1967.
- [5] S. B. Weinstein and P. M. Ebert, “Data transmission by frequency division multiplexing using the discrete Fourier transform,” *IEEE Trans. on Commun.*, vol. 19, pp. 628–634, Oct. 1971.
- [6] A. C. Bingham, “Multicarrier modulation for data transmission: An idea whose time has come,” *IEEE Commun. Magazine*, pp. 5–14, May 1990.

- [7] A. Peled and A. Ruiz, “Frequency domain data transmission using reduced computational complexity algorithms,” *Proc. of International Conf. on Acoustics, Speech, and Signal Processing*, pp. 964–967, 1980.
- [8] B. Hirosaki, “An orthogonally multiplexed QAM system using the discrete Fourier transform,” *IEEE Trans. on Commun.*, vol. 29, pp. 982–989, July 1981.
- [9] R. V. Nee and R. Prasad, *OFDM For Wireless Multimedia Communications*, Artech House, Jan. 2000.
- [10] I. J. Cimini Jr., “Analysis and simulation of a digital mobile channel using orthogonal frequency division multiplexing,” *IEEE Trans. on Commun.*, vol. 33, pp. 665–673, July 1985.
- [11] ETSI, “Digital video broadcasting: Framing structure, channel coding, and modulation for digital terrestrial television,” ETS 300-744, Aug. 1997.
- [12] ETSI, “Radio broadcasting systems: Digital audio broadcasting (DAB) to mobile, portable, and fixed receivers,” ETS 300 401 ed.2, May 1997.
- [13] J. C. Rault, D. Castelain, and B. L. Floch, “The coded orthogonal frequency division multiplexing (COFDM) technique, and its application to digital radio broadcasting towards mobile receivers,” *Proc. of Global Telecommun. Conf.*, pp. 428–432, Nov. 1989.

- [14] M. Russel and G. L. Stuber, "Terrestrial digital video broadcasting for mobile reception using OFDM," *Wireless Personal Commun.*, vol. 2, pp. 45–66, 1995.
- [15] L. Thibault and M. T. Le, "Performance evaluation of COFDM for digital audio broadcasting part i: Parametric study," *IEEE Trans. on Broadcasting*, vol. 43, pp. 64–75, Mar. 1997.
- [16] J. A. C. Bingham, *ADSL, VDSL, and Multicarrier Modulation*, New York Wiley, 2000.
- [17] P. S. Chow, J. C. Tu, and J. M. Cioffi, "Performance evaluation of a multichannel transceiver system for ADSL and VHDSL services," *IEEE Journal on Selected Areas in Commun.*, vol. 9, pp. 909–919, Aug. 1991.
- [18] D. C. Jones, "Frequency domain echo cancellation for discrete multi-tone aysmmetric digital subscriber line transceivers," *IEEE Trans. on Commun.*, vol. 43, pp. 1663–1672, Feb./Mar./Apr. 1995.
- [19] H. Sari and G. Karam, "Orthogonal frequency division multiple access and its application to CATV network," *European Trans. on Commun.*, vol. 9, pp. 507–516, Dec. 1998.
- [20] IEEE 802.11, "IEEE standard for wireless lan medium access control (MAC) and physical layer (PHY) specifications," Nov. 1997.

- [21] B. P. Crow, I. Widjada, J. G. Kim, and P. T. Sakai, "IEEE 802.11 wireless local area networks," *IEEE Commun. Magazine*, pp. 116–126, Sept. 1997.
- [22] ETSI, "Radio equipment and systems high performance radio local area network (HIPERLAN) type 1," ETS, 300-652, Oct. 1996.
- [23] ETSI, "Broadband radio access networks (BRAN); HIPERLAN type 2 technical specification part i-physical layer," DTS/BRAN030003-1, Oct. 1999.
- [24] R. Van Nee, G. Awater, M. Morikura, H. Takanashi, M. Webster, and K. W. Halford, "New high-rate wireless lan standards," *IEEE Commun. Magazine*, pp. 82–88, Dec. 1999.
- [25] D. Gerakoulis and P. Salmi, "An interference suppressing OFDM system for ultra wide bandwidth radio channels," *Proc. of IEEE Conf. on Ultra Wideband Systems and Technologies.*, pp. 259–264, May 2002.
- [26] E. Saberinia and A. H. Tewfik, "Generating UWB-OFDM signal using sigma-delta modulator," *Proc. of IEEE Vehicular Technology Conference*, pp. 1425–1429, April 2003.
- [27] Y. Kim, B. Jeong, J. Chung, C. Hwang, J. Ryu, K. Kim, and Y. Kim, "Beyond 3G: Vision, requirements, and enabling technologies," *IEEE Commun. Mag.*, pp. 120–124, Mar. 2003.

- [28] V. Tarokh, N. Seshadri, and A. R. Calderbank, "Space-time codes for high data rate wireless communication: Performance criterion and code construction," *IEEE Trans. on Inform. Theory*, vol. 44, pp. 744–765, Mar. 1998.
- [29] A. F. Naguib, N. Seshadri, and A. R. Calderbank, "Increasing data rate over wireless channel," *IEEE Signal Processing Magazine*, vol. 17, pp. 76–92, May 2000.
- [30] V. Tarokh, H. Jafarkhani, and A. R. Calderbank, "Space-time block codes from orthogonal designs," *IEEE Trans. on Inform. Theory*, vol. 5, pp. 1456–1467, July 1999.
- [31] V. Tarokh, H. Jafarkhani, and A. R. Calderbank, "Space-time block coding for wireless communications : Performance results," *IEEE Journal on Selected Areas in Commun.*, vol. 17, pp. 451–460, Mar. 1999.
- [32] X. Li, T. Luo, G. Yue, and C. Yin, "A squaring method to simplify the decoding of orthogonal space-time block codes," *IEEE Trans. on Commun.*, vol. 49, pp. 1700–1703, Oct. 2001.
- [33] S. M. Alamouti, "A simple transmit diversity technique for wireless communications," *IEEE Journal on Selected Areas in Commun.*, vol. 16, pp. 1451–1458, Oct. 1998.
- [34] D. Agrawal, V. Tarokh, A. Naguib, and N. Seshadri, "Space-time coded OFDM for high data-rate wireless communication over wideband chan-

- nels,” *Proc. of Vehicular Technology Conf.*, vol. 3, pp. 2232–2236, May 1998.
- [35] B. Lu and X. Wang, “Space-time code design in OFDM systems,” *Proc. of Global Telecommun. Conf.*, vol. 2, pp. 1000–1004, Dec. 2000.
- [36] M. Russell and G. L. Stuber, “Interchannel interference analysis of OFDM in a mobile environment,” *Proc. of Vehicular Technology Conf.*, vol. 2, pp. 25–28, July 1995.
- [37] H. Cheon and D. Hong, “Performance analysis of space-time block codes in time-varying Rayleigh fading channels,” *Proc. of International Conf. on Acoustics, Speech, and Signal Processing*, vol. 3, pp. 2357–2360, May 2002.
- [38] A. Stamoulis, S. N. Diggavi, and N. Al-Dhahir, “Intercarrier interference in MIMO OFDM,” *IEEE Trans. on Signal Porcessing*, vol. 50, pp. 2451–2464, Oct. 2002.
- [39] Z. Liu, X. Ma, and G. B. Giannakis, “Space-time coding and Kalman filtering for time-selective fading channels,” *IEEE Trans. on Commun.*, vol. 2, pp. 183–186, Feb. 2002.
- [40] T. A. Tran and A. B. Sesay, “A generalized simplified ML decoder of orthogonal space-time block code for wireless communications over time-selective fading channels,” *Proc. of Vehicular Technology Conf.*, pp. 1911–1915, Sept. 2002.

- [41] W. M. Younis, N. Al-Dhahir, and A. H. Sayed, "Adaptive frequency-domain equalization of space-time block-coded transmissions," *Proc. of International Conf. on Acoustics, Speech, and Signal Processing*, vol. 3, pp. 2353–2356, May 2002.
- [42] Y. Gong and K. B. Lataief, "An efficient space-frequency coded wide-band OFDM system for wireless communications," *Proc. of International Conf. on Commun.*, vol. 1, pp. 475–479, May 2002.
- [43] Y. Sun and L. Tong, "Channel equalization for wireless OFDM systems with ICI and ISI," *Proc. of International Conf. on Commun.*, vol. 1, pp. 182–186, June 1999.
- [44] S. N. Diggavi, N. Al-Dhahir, A. Stamoulis, and A. R. Calderbank, "Differential space-time coding for frequency-selective channels," *IEEE Commun. Letters*, vol. 6, pp. 253–255, June 2002.
- [45] J. F. Hayes, "The viterbi algorithm applied to digital data transmission," *IEEE Commun. Magazine*, vol. 40, pp. 26–32, May 2002.
- [46] J. P. Seymour and M. P. Fitz, "Near-optimal symbol-by-symbol detection schemes for flat Rayleigh fading," *IEEE Trans. on Commun.*, vol. 43, pp. 1525–1533, Feb./Mar./April 1995.
- [47] W. Jeon, K. Chang, and Y. Cho, "An equalization technique for orthogonal frequency division multiplexing systems in time-variant multipath channels," *IEEE Trans. on Commun.*, vol. 1, pp. 27–32, Jan. 1999.

- [48] Ye Li, “Simplified channel estimation for OFDM systems with multiple transmit antennas,” *IEEE Trans. on Wireless Commun.*, vol. 1, pp. 67–75, Jan. 2002.
- [49] H. Minn, D. I. Kim, and V. Bhargava, “A reduced complexity channel estimation for OFDM systems with transmit diversity in mobile wireless channels,” *IEEE Trans. on Commun.*, vol. 50, pp. 799–807, May 2002.
- [50] S. Mudulodu and A. Paulraj, “A transmit diversity scheme for frequency selective fading channels,” *Proc. of Global Telecommun. Conf.*, vol. 2, pp. 1089–1093, Dec. 2000.
- [51] W. C. Jakes, *Microwave Mobile Communications*, Willey, 1974.
- [52] J. Kim, B. Jang, R. W. Heath Jr., and E. J. Powers, “A decision directed receiver for OFDM systems with transmit diversity,” *Accepted to Vehicular Technology Conference*, Oct. 2003.
- [53] J. Kim, R. W. Heath Jr., and E. J. Powers, “A decision directed receiver for Alamouti coded OFDM systems,” *IEICE Trans. on Commun.*, vol. e86-b, pp. 3141–3143, Oct. 2003.
- [54] J. Kim, R. W. Heath Jr., and E. J. Powers, “A symbol estimation scheme for Alamouti coded OFDM systems,” *Accepted to Military Commun. Conf.*, Oct. 2003.

- [55] J. Kim, R. W. Heath Jr., and E. J. Powers, “Receiver designs for alamouti coded OFDM systems in fast fading channels,” *Accepted for IEEE Trans. on Wireless Commun.*
- [56] A. Duel-Hallen and C. Heegard, “Delayed decision-feedback sequence estimation,” *IEEE Trans. on Commun.*, vol. 37, pp. 428–436, May 1989.
- [57] W. Gerstacker and R. Schober, “Equalization concepts for edge,” *IEEE Trans. on Wireless Commun.*, vol. 1, pp. 190–199, Jan. 2002.
- [58] S. J. Simmons, “Breadth-first trellis decoding with adaptive effort,” *IEEE Trans. on Commun.*, vol. 38, pp. 3–12, Jan. 1990.
- [59] H. Zamiri-Jafarian and S. Pasupathy, “Complexity reduction of the MLSD/MLSDE receiver using the adaptive state allocation algorithm,” *IEEE Trans. on Wireless Commun.*, vol. 1, pp. 101–111, Jan. 2002.
- [60] Y. Choi, P. J. Voltz, and F. A. Cassara, “On channel estimation and detection for multicarrier signals in fast and selective Rayleigh fading channels,” *IEEE Trans. on Commun.*, vol. 49, pp. 1375–1387, Aug. 2001.
- [61] J. Kim and E. J. Powers, “Reduced complexity signal detection for OFDM systems with transmit diversity,” *In preparation for IEEE Trans. on Vehicular Technology.*
- [62] J. W. Demmel, *Applied Numerical Linear Algebra*, SIAM, 1997.

- [63] J. Kim, J. Kang, and E. J. Powers, "A bandwidth efficient OFDM transmission scheme," *Proc. of International Conf. on Acoustics, Speech, and Signal Processing*, pp. 2329–2332, May 2002.
- [64] D. Kim and G. L. Stuber, "Residual isi cancellation for OFDM with application to HDTV broadcasting," *IEEE Journal on Selected Areas in Commun.*, vol. 16, pp. 1590–1599, Oct. 1998.
- [65] A. M. Saleh and R. A. Valenzuela, "A statistical model for indoor multipath propagation," *IEEE J. Selected Areas in Comm.*, pp. 128–137, Feb. 1987.
- [66] J. Kim, E. J. Powers, and Y. Cho, "A non-synchronized sampling scheme," *Proc. of the 36th Asilomar Conference on Signals, Systems, and Computers*, Nov. 2002.
- [67] T. Pollet, P. Spruyt, and Moeneclaey, "The ber performance of OFDM systems using non-synchronized sampling," *Proc. Global Telecommun. Conf.*, pp. 253–257, Dec. 1994.
- [68] T. Pollet and M. Peeters, "Synchronization with DMT modulation," *IEEE Commun. Mag.*, pp. 80–86, April 1999.
- [69] T. Pollet and M. Peeters, "A new digital timing correction scheme for DMT systems," *Proc. of International Conf. on Commun.*, pp. 1805–1808, June 2000.

- [70] C. Y. Wong, R. S. Cheng, K. B. Letaief, and R. D. Murch, "Multiuser OFDM with adaptive subcarrier, bit, and power allocation," *IEEE Journal on Selected Areas in Commun.*, vol. 17, pp. 1747–1758, Oct. 1999.
- [71] D. Kivanc, G. Li, and H. Liu, "Computationally efficient bandwidth allocation and power control for ofdma," *IEEE Trans. on Wireless Commun.*, vol. 2, pp. 1150–1158, Nov. 2003.
- [72] P. Xia, S. Zhou, and G. B. Giannakis, "Bandwidth and power efficient multicarrier multiple access," *IEEE Trans. on Commun.*, vol. 51, pp. 1828–1837, Nov. 2003.
- [73] R. S. Cheng and S. Verdu, "Gaussian multiaccess channels with isi: Capacity region and multiuser water-filling," *IEEE Trans. on Info. Theory*, vol. 39, pp. 773–785, May 1993.
- [74] D. N. Tse and S. V. Hanly, "Multiaccess fading channels - part i: Polymatroid structure, optimal resource allocation and throughput capacities," *IEEE Trans. on Info. Theory*, vol. 44, pp. 2796–2815, Nov. 1998.
- [75] IEEE 802.16a, "Standard for local and metropolitan area networks part 16: Air interface for fixed broadband wireless access systems - amendments 2: Medium access control modifications and additional physical layer specifications for 2-11 ghz," 2003.
- [76] C. Eklund, R. B. Marks, K. Stanwood, and S. Wang, "IEEE standard 802.16: A technical overview of the wirelessman air interface for broadband," 2003.

- band wireless access,” *IEEE Commun. Magazine*, pp. 98–107, June 2002.
- [77] Israel Koffman and V. Roman, “Broadband wireless access solutions based on OFDM access in IEEE 802.16,” *IEEE Commun. Magazine*, pp. 96–103, April 2002.
- [78] D. Gesbert, M. Shafi, D. Shiu, P. Smith, and A. Naguib, “From theory to practice: An overview of MIMO space-time coded wireless systems,” *IEEE Journal on Selected Areas in Commun.*, vol. 21, pp. 281–302, April 2003.
- [79] W. Younis and N. Al-Dhahir, “Joint prefiltering and MLSE equalization of space-time-coded transmissions over frequency-selective channels,” *IEEE Trans. on Vehicular Technology*, vol. 51, pp. 144–154, Jan. 2002.
- [80] M. Toeltsch and A. F. Molisch, “Efficient OFDM transmission without cyclic prefix over frequency-selective channels,” *IEEE International Symposium on Personal, Indoor and Mobile Radio Commun.*, vol. 2, pp. 1363–1367, Sept. 2000.
- [81] M. H. Hayes, *Statistical Digital Signal Processing and Modelling*, John Wiley & Sons, 1996.
- [82] Z. Wang and G. B. Giannakis, “Wireless multicarrier communications,” *IEEE Signal Processing Magazine*, pp. 29–48, May 2000.

- [83] W. Jeon, “A study on the compensation of nonlinear distortion, equalization, and synchronization techniques for OFDM systems,” *Ph.D. Dissertation, Chung-Ang University, Seoul, South Korea*, June 1999.

Vita

Jaekwon Kim, a son of Shin-Hwan Kim and Jung-Rye Cho, was born in 1972, Youngkwang, Junnam, South Korea. Jaekwon Kim received B.S. degree with graduation ranking of 1/103 from Chung-Ang University in Electrical Engineering, Seoul, South Korea in 1995. From June 1996 to August 1998, he served as a soldier in personnel management department, Kangwon, South Korea. He obtained M.S. degree from Chung-Ang University in Electrical Engineering in 2000. During his master's program, he conducted research on equalization and synchronization for $xDSL$ systems. He started the Ph.D. program in September 2000 at the Department of Electrical and Computer Engineering, The University of Texas at Austin. He is a member of the Wireless Networking and Communications Group (WNCG), The University of Texas at Austin, where he focuses his research on signal detection for multi-carrier systems under harsh channel environments due to either high Doppler or long channel impulse responses. He won the Texas Telecommunications Engineering Consortium (TexTEC) Fellowship twice, Fall 2001-Spring 2002 and Fall 2002-Spring 2003.

Permanent address: 356 Jangdong, Chunkdong 1-ku, Yumsan,
Youngkwang, Junnam, South Korea.

This dissertation was typeset with \LaTeX^\dagger by the author.

[†] \LaTeX is a document preparation system developed by Leslie Lamport as a special

version of Donald Knuth's T_EX Program.